Predicting the Bifurcation Structure of Localized Snaking Patterns

Elizabeth Makrides
Division of Applied Mathematics
Brown University
Providence, RI 02912, USA

Björn Sandstede
Division of Applied Mathematics
Brown University
Providence, RI 02912, USA

March 28, 2013

Abstract

We expand upon a general framework for studying the bifurcation diagrams of localized spatially oscillatory structures. Building on work by Beck *et al.*, the present work provides an analytical explanation for the numerical results of Houghton and Knobloch on symmetry breaking in systems with one spatial dimension, and makes predictions on the effects of symmetry breaking in more general settings, including planar systems. In particular, we predict analytically, and subsequently confirm numerically, the formation of isolas upon particular symmetry breaking perturbations. While our numerical results involve continuation of planar stripe and spot solutions in the Swift–Hohenberg model system, we emphasize the general applicability of the analytical results.

1 Introduction

Localized structures, in which a spatially oscillatory pattern on a finite spatial range connects to a trivial homogeneous solution outside this range, have been observed in numerous physical systems [1, 4, 5, 11, 20]; see also [2, 13] for additional references. The bifurcation diagrams of such patterns often exhibit snaking behavior, in which a branch of symmetric solutions winds back and forth between two limits of an appropriate parameter, allowing for patterns of arbitrary spatial extent [6, 10, 14, 21, 22, 25]. Asymmetric solution branches connecting symmetric snaking branches were discovered numerically in [7, 8], using the Swift–Hohenberg model system in one dimension. The origin of the symmetric and asymmetric solution branches was explained under general hypotheses in [3], and near a certain codimension-two point in [9, 17].

While the appearance of snaking is now generally well understood, it remains of interest to understand the behavior of solutions under different assumptions, including the structure of bifurcation diagrams under perturbations to the governing equation. One characteristic common to many snaking systems is spatial reversibility, and we assume throughout that our systems possess this property; we note that the behavior of systems without such reversibility was recently explored in [23] as well as [16]. In addition, many physical systems of interest contain a $\mathbb{Z}_2$ symmetry, corresponding, for example, to symmetry in the midplane of a fluid system. In the present work we illustrate how a general approach to localized structures can be leveraged to predict and understand the effects of perturbations breaking this additional symmetry. This question was recently explored numerically in [15] for the one-dimensional Swift–Hohenberg model. Here we follow up on the results of [3] to show that the effects of perturbative symmetry breaking terms on particular solution types and overall bifurcation structure are fully predictable analytically. In addition to explaining previously published numerical findings, we use these methods to predict new bifurcation structures, including the formation of isolas upon the introduction of appropriate symmetry breaking terms. We then confirm these predictions numerically for a planar system.

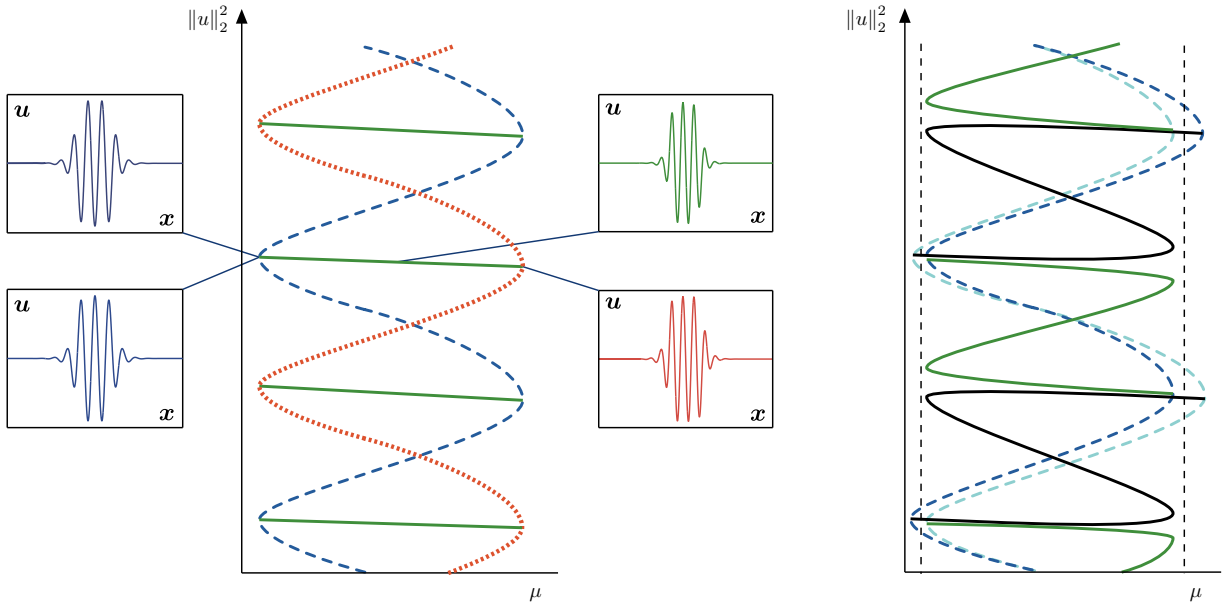

Figure 1: Left: *Schematic of the bifurcation diagram for the unperturbed system (2.1) with $\varepsilon = 0$, with illustrative solution profiles. The dashed dark blue snaking branch consists of two branches of even parity solutions, while the dotted orange branch consists of two branches of odd parity solutions. Solid green cross-connecting branches consist of four sets of asymmetric solutions.* Right: *Schematic of the bifurcation diagram for a perturbed system as in (2.1) with $\varepsilon \neq 0$. Snaking branches for even symmetric patterns with central maximum and minimum are shown in dark and light blue dashed, respectively. Asymmetric branches are in solid black and green. Dashed vertical lines indicate the saddle node locations from the unperturbed system.*

Though we use the Swift–Hohenberg equation to demonstrate our results numerically, we wish to emphasize that the hypotheses we impose are not specific to the Swift–Hohenberg setting. In particular, as shown in [3], we do not require the system to be conservative when posed as a spatial dynamical system, meaning that the underlying PDE system need not be variational. Furthermore, while we have focused on symmetry-breaking terms, this approach is applicable to any perturbative terms preserving spatial reversibility.

The paper is organized as follows: in Section 2, we review the numerical results of Houghton and Knobloch [15] on symmetry breaking in the 1D Swift–Hohenberg model, which initiated the present work. In Section 3, we link the framework introduced in [3] with a formal gluing approach of fronts and backs, first to indicate the broad applicability of the approach taken in [3] and, second, to understand some of the major features observed in systems admitting localized patterns. We note that this section is intended to provide intuition and motivate the particular hypotheses employed in the following section, rather than to present precise results for a particular system. In Section 4, we detail predictions on the evolution of bifurcation diagrams upon the introduction of perturbative symmetry breaking terms. In Section 5 we provide numerical continuation studies on planar stripe and spot patterns, studied previously in [2]; these numerical results confirm our analytical predictions from Section 4, including the existence of isolas produced by the rearrangement of odd-symmetric and asymmetric solution branches. We also explain and illustrate how the full bifurcation diagram for a wide variety of perturbations can be obtained from the bifurcation diagram of an unperturbed system, without actually carrying out the numerical continuation. Finally, in Section 6 we identify areas for future work.

2 Existing numerical results

Current knowledge regarding the effects of symmetry breaking in spatially localized oscillatory solutions comes from a recent paper [15] of Houghton and Knobloch, employing numerical continuation methods to the one-dimensional cubic-quintic Swift–Hohenberg model. In particular, they examine[1] the variational system

$$u_t = -(1+\partial_x^2)^2 u - \mu u + \nu u^3 - u^5 + \varepsilon u^2 \tag{2.1}$$

as well as the non-variational system

$$u_t = -(1+\partial_x^2)^2 u - \mu u + \nu u^3 - u^5 + \varepsilon (\partial_x u)^2 \tag{2.2}$$

for $0 < \varepsilon \ll 1$.

The one-dimensional unperturbed cubic-quintic Swift–Hohenberg equation with $\varepsilon = 0$ has been studied extensively. This system is equivariant under the $\mathbb{Z}_2$ symmetry $u \mapsto -u$. The left-hand side of Figure 1 provides a schematic of its bifurcation diagram, along with sample solution profiles. We note that the snaking branch in dashed dark blue consists of two solution branches lying on top of each other in the $(\mu, \|u\|_2^2)$ plane, one consisting of symmetric solutions with a central maximum and the other one of symmetric solutions with a central minimum: these two solution profiles are transformed into each other by the symmetry $u \mapsto -u$. Similarly, the dotted orange snaking branch is actually two branches of odd parity solutions related again by the $u \mapsto -u$ symmetry. Finally, each asymmetric ladder branch is a set of four solution branches, which coincide in the $(\mu, \|u\|_2^2)$ plane. Moving up along a snaking branch, localized structures grow by increasing the extent of the spatially periodic region between the trivial homogeneous state.

Once ε becomes nonzero in either (2.1) or (2.2), the system no longer respects the symmetry $u \mapsto -u$, and the right-hand side of Figure 1 provides a schematic of the resulting bifurcation diagram for (2.1) with $\varepsilon \neq 0$. Houghton and Knobloch observe that the even solutions persist along unbroken snaking branches: however, in contrast to the $\varepsilon = 0$ case, the two snaking branches for the even symmetric solutions with, respectively, a central maximum and a central minimum no longer lie on top of each other due to the broken $\mathbb{Z}_2$ symmetry. Meanwhile the odd solutions are destroyed, and two types of asymmetric solution branches are formed, termed S and Z branches in accordance with their shapes. The Z branches start and end on the same symmetric branch, whereas the S branches connect the two symmetric solution branches to each other.

It is also observed that, after symmetry breaking, alternate saddle nodes on the left and right are offset to the inside and outside of the original branches, so that the resulting bifurcation diagram possesses four snaking limits. Finally, Houghton and Knobloch comment that the saddle nodes on the right undergo larger displacement as compared to those on the left.

In the following, we provide both an intuitive framework and rigorous results to demonstrate how these numerical findings can be anticipated analytically. Furthermore, we generalize these findings to planar systems, as well as to governing equations which may be more appropriate for describing particular physical systems.

3 General framework

Our aim in this section is to relate the rigorous analysis and its underlying framework developed in [3] with a formal approach that views the emergence of localized roll patterns via gluing together appropriate building blocks consisting of fronts and backs. Outlining this connection should indicate the broad applicability of the results in [3] without expanding on the technical account in that paper. The link between these two different approaches will also enable us to predict the effects of symmetry-breaking perturbations more easily in the forthcoming sections.

[1] We remark that Houghton and Knobloch use the bifurcation parameter $r := -\mu$ instead of μ: hence, their bifurcation diagrams are flipped in comparison to ours; in our description of their results, we use μ as the parameter.

3.1 Basic assumptions

First, we will provide an intuitive treatment of the realization of localized roll patterns from simpler building blocks. In this spirit, rather than specifying a form for the PDE or ODE governing our system of interest, we make the basic assumption that the system admits fronts, i.e., solutions evolving from a constant state to a spatially oscillatory one. More precisely, if we write stationary solutions as $u(x) \in \mathbb{R}^n$ with $x \in \mathbb{R}$, we assume that there exist steady states $u_f(x)$ such that $u_f(x) \to u_0$ as $x \to -\infty$ and $u_f(x) \to v(x)$ as $x \to +\infty$, where $v(x)$ is periodic in x with nonzero minimal period. In fact, we can more generally consider systems admitting solutions $u_f(x, y)$, where $y \in \Omega \Subset \mathbb{R}^{d-1}$, which satisfy $u_f(x, y) \to w(y)$ as $x \to -\infty$, where $w(y)$ is any function independent of x, as well as $u_f(x, y) \to v(x, y)$ as $x \to +\infty$, where $v(x, y)$ is periodic in x. In essence we require only that the evolution in space occur along one dimension, perhaps after an appropriate coordinate transformation. For simplicity in this section we write solutions as $u(x)$, but in subsequent sections we will use the more general formulation to predict some interesting effects of symmetry breaking, including the formation of isolas in planar systems under appropriate conditions, and to verify these predictions numerically.

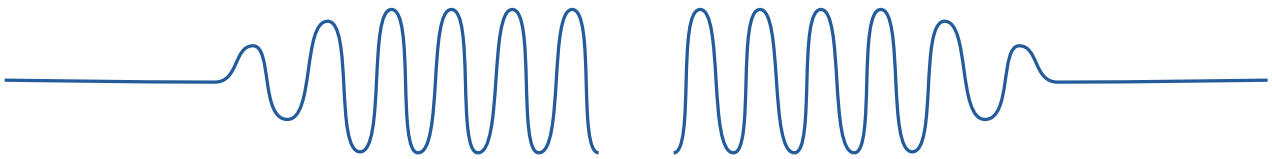

$u_f(x)$, a front $\qquad\qquad$ $u_b(x) = u_f(-x)$, a back

Figure 2: *Illustration of a front and a back, related by $x \mapsto -x$.*

We will assume throughout that our system is reversible in the front evolution variable. With the above notation, this means we have $x \mapsto -x$ symmetry, so that given any solution $u(x)$, $u(-x)$ is also a solution. In the case that $u_f(x)$ is a front, $u_b(x) := u_f(-x)$ is termed a back; see Figure 2. The periodic orbit $v(x)$ approached by fronts is assumed to be invariant under $x \mapsto -x$.

Our primary interest will be in systems that have an additional $\mathbb{Z}_2$ symmetry κ, and in Section 4 we will describe the results of breaking this symmetry in a perturbative manner. Consequently, in the following we will look to understand the characteristics of systems with and without the $\mathbb{Z}_2$ symmetry κ. For concreteness, in this section we will assume the symmetry is $\kappa : u \mapsto -u$, and in this case further assume that the constant solution approached as $x \to \pm\infty$ is $u_0 = 0$. We will finally assume that the limiting oscillatory solution $v(x)$ is compatible with the κ symmetry, which implies that $-v(x) = v(x+\pi)$. Then, given a front solution $u_f(x)$, we will also have the front solution $u_{f2}(x) := -u_f(x)$, as well as the back solutions $u_{b1}(x) := u_f(-x)$ and $u_{b2}(x) := -u_f(-x)$.

3.2 Construction of localized solutions via gluing

We now wish to "glue" together front and back solutions to form a localized stationary solution $u_{loc}(x)$ which is invariant under $u(x) \mapsto u(-x)$. Clearly this is only possible if we have a maximum or minimum at the center of the localized oscillatory structure. Defining the phase φ at the center of the localized solution to be the distance traveled past a maximum, and rescaling x if necessary so that the spatially oscillatory limiting solution $v(x)$ mentioned above has period 2π, this is equivalent to requiring that the phase at the center of the structure satisfies $\varphi = 0$ or $\varphi = \pi$; see Figure 3.

In the case that we have the additional symmetry $\kappa : u \mapsto -u$, we recall that the existence of a front solution $u_f(x)$ implies the existence of the front solution $u_{f2}(x) := -u_f(x)$ and the back solutions $u_{b1}(x) := u_f(-x)$ and

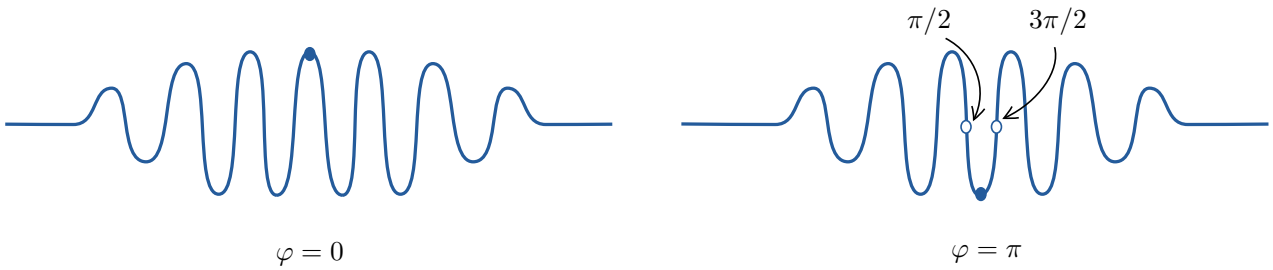

Figure 3: *Possible phases $\varphi = 0, \pi$ for a localized solution invariant under $x \mapsto -x$. The closed circles indicate the midpoint of the pattern, while the labels $\frac{\pi}{2}$ and $\frac{3\pi}{2}$ indicate the value of φ at the open circles.*

$u_{b2}(x) := -u_f(-x)$. Thus we can form solutions invariant under $u(x) \mapsto -u(-x)$ by gluing a front $u_f(x)$ to a back $u_{b2} = -u_f(-x)$ with phase $\varphi = \frac{\pi}{2}$ or $\varphi = \frac{3\pi}{2}$; see Figure 4.

Figure 4: *Solutions invariant under $u(x) \mapsto -u(-x)$, with phases $\varphi = \frac{\pi}{2}, \frac{3\pi}{2}$.*

Moving forward, we will refer to solutions invariant under $u(x) \mapsto u(-x)$ as symmetric, or $\mathcal{R}$-symmetric. In the case that the system possesses the additional $\kappa : u \mapsto -u$ symmetry, we will also refer to solutions invariant under $u(x) \mapsto -u(-x)$ as symmetric, or $\kappa\mathcal{R}$-symmetric. Any localized solution which is not invariant under either of these operations will be called asymmetric.

3.3 Solution lengths and parameter dependence

To this point, we have not considered the role of parameters in our system. If we only had one "type" of front present, which is to say all front solutions could be mapped to each other via a translation in x, then we would only be able to get symmetric localized states in lengths of multiples of 2π (or, if $u \mapsto -u$ symmetry is present, in multiples of π); see Figure 5. If, however, we can define a characteristic length of fronts such that the length of the fronts present in our system varies continuously with a parameter, then our system will typically admit localized symmetric solutions of arbitrary length via parameter variation.

We pause here to consider the notion of length. Although there is a natural and rigorous way to measure these lengths in a dynamical systems setting, using Poincarè sections near the oscillatory solution, we will not aim at fully rigorous definitions and instead suggest an approximate measurement using only the solution profiles. Specifically, we will make use of two distinct lengths: first, the *length of a localized structure* is the extent of the region where our localized solution lies near the oscillatory solution. We will generally denote this by $2\bar{L}$, since we are usually interested in half this length. To measure the length of a localized oscillatory solution, we can look at the difference between the largest x, called x_1 in Figure 5, such that $u_{loc}(x)$ is within some tolerance of the constant solution, and the smallest x, called x_2 in Figure 5, such that it is again within this tolerance. Alternatively, assuming $u_0 = 0$, we can use the L^2 norm of the whole localized solution. The former

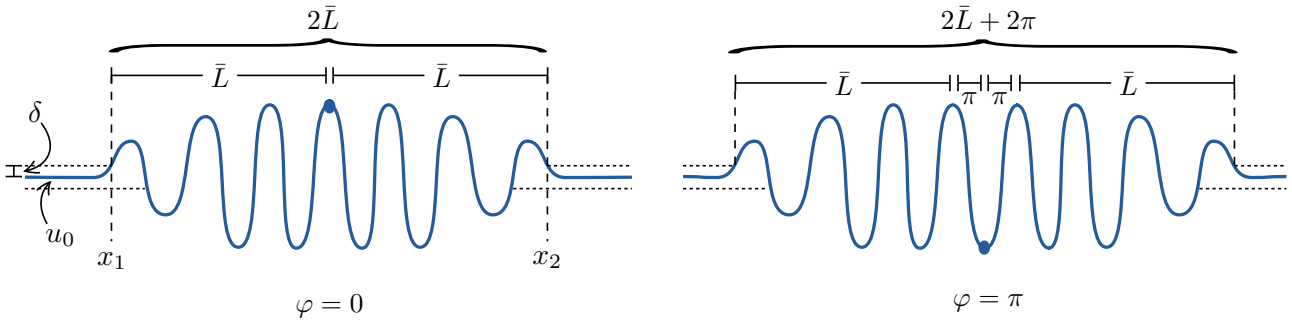

Figure 5: *The length of a localized structure, measured as the distance between the largest x, labeled x_1, such that $|u(x) - u_0| < \delta$ for all $x < x_1$, and the smallest x, labeled x_2 such that $|u(x) - u_0| < \delta$ for all $x > x_2$, for some fixed tolerance δ.*

measurement is more natural for theoretical development, while the latter is more convenient for numerically computed bifurcation diagrams, but fundamentally both capture the same information.

Second, the *characteristic length of a front*, which we denote by l and define modulo 2π, corresponds to the length of the interface region between the constant and oscillatory solution measured to a peak, modulo 2π [2]. That is, we look at the difference between the largest x such that $u_{loc}(x)$ is within some tolerance of the constant solution to the smallest x corresponding to a peak (i.e., $u'(x) = 0$, $u''(x) < 0$) within some tolerance of the amplitude of the limiting oscillatory solution $v(x)$; see Figure 6. Again, assuming $u_0 = 0$, we can also measure this via the L^2 norm of the portion of a front lying to the left of an oscillatory peak within some tolerance of the maximum amplitude.

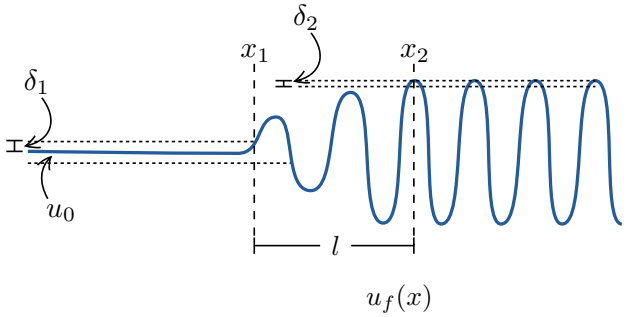

Figure 6: *The characteristic length of a front for some fixed tolerances δ_1 and δ_2, measured as the distance between the largest x, labeled x_1, such that $|u(x) - u_0| < \delta_1$ for all $x < x_1$, and the smallest x, labeled x_2, such that $u'(x_2) = 0$, $u''(x_2) < 0$, and $|u(x_2) - v(x_*)| < \delta_2$, where $v(\cdot)$ is the limiting oscillatory solution, and $v(x_*)$ has phase $\varphi = 0$.*

Having established these two types of length, and approximately how to measure them, we finally wish to include dependence on a system parameter μ. In general, fronts will come locally in branches (smooth solution curves) as the only steady-state bifurcations they typically undergo in 1-parameter systems are saddle node bifurcations (possibly after ignoring bifurcations caused by symmetry breaking in the transverse y-direction.) If we assume that fronts exist only for $\mu \in (\mu_1, \mu_2)$, then plotting (μ, l) along the branch of fronts, we obtain typical bifurcation or existence diagrams as shown in Figure 7. On the cylinder $(\mu_1, \mu_2) \times S^1$ (recall the characteristic length l of fronts is taken modulo 2π), the connected branch containing our front solution can have any one of these forms, as well as others not shown in Figure 7.

[2]Note that we are assuming all fronts connect to oscillatory solutions with the same period, which we normalize without loss of generality to 2π.

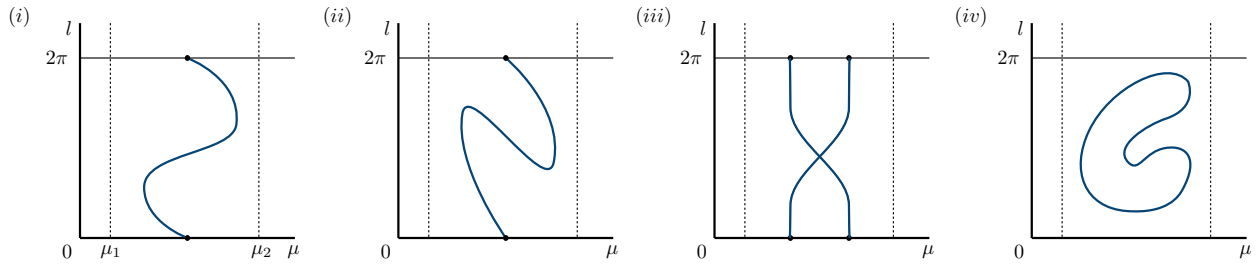

Figure 7: *Typical bifurcation and existence diagrams for fronts on $(\mu_1, \mu_2) \times S^1$, where l is the characteristic length of fronts and μ is a system parameter.*

Though the approach outlined below applies to all of these, we will assume for the sake of clarity that each l corresponds to a unique μ, so that the branch on $(\mu_1, \mu_2) \times S^1$ can be written as $\mu = z(l)$ with $l \in [0, 2\pi]/\sim$ for some function z, as illustrated in Figure 7(i). We can extend the function z to all of $\mathbb{R}$ by considering the argument modulo 2π. We will generally write $z(L)$ to indicate the extended version.

3.4 Bifurcation structure of localized solutions assuming only $x \mapsto -x$ symmetry

Now suppose we have a symmetric localized structure of length $2\bar{L}$ with maximum in the center, i.e., with phase $\varphi = 0$. Such a structure may be formed from a front of characteristic length $l = \bar{L} \bmod 2\pi$ and a back of the same characteristic length, so that such a solution exists for $\mu = z(\bar{L})$. On the other hand, a symmetric localized structure of length $2\bar{L}$ with minimum in the center (phase $\varphi = \pi$) is formed from a front of characteristic length $(\bar{L} - \pi) \bmod 2\pi$ and a back of characteristic length $(\bar{L} + \pi) \bmod 2\pi$, so that such a solution exists for $\mu = z(\bar{L} + \pi)$; recall here that z is 2π-periodic so that $z(\bar{L} + \pi) = z(\bar{L} - \pi)$. Consequently, in a bifurcation diagram displaying the length (L^2 norm) of a localized solution versus parameter μ, the curve $\mu = z(\bar{L})$ will be the branch of symmetric localized solutions with maxima in the center, while the branch of solutions with minima in the center will be given by $\mu = z(\bar{L} + \pi)$. The resulting bifurcation diagram of symmetric branches for z as given in Figure 7(i) therefore consists of snaking branches which are intertwined in the sense of Figure 1.

Turning to asymmetric solutions, suppose we have a localized structure of length $2\bar{L}$, and again define the phase φ at the midpoint to be the distance past the nearest maximum on the left. Such a structure is formed from a front of characteristic length $(\bar{L} - \varphi) \bmod 2\pi$ and a back of characteristic length $(\bar{L} + \varphi) \bmod 2\pi$; see Figure 8.

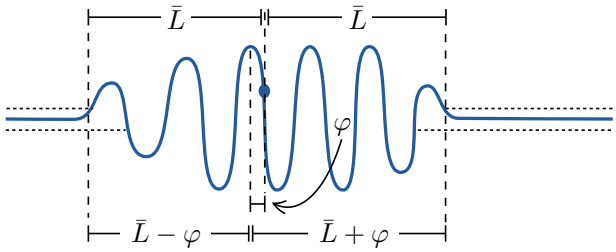

Figure 8: *An asymmetric localized structure of length $2\bar{L}$, which can be viewed as the result of combining a front of characteristic length $\bar{L} - \varphi$ with a back of characteristic length $\bar{L} + \varphi$, where φ is the phase at the midpoint of the localized structure.*

Thus we can have a localized structure of length $2\bar{L}$ and phase φ if and only if $\mu = z(\bar{L} + \varphi)$ and $\mu = z(\bar{L} - \varphi)$,

requiring in particular that $z(\bar{L}+\varphi) = z(\bar{L}-\varphi)$. In other words, a localized structure of length $2\bar{L}$ can exist at a particular μ if and only if there exists a φ such that $\mu = z(\bar{L}+\varphi) = z(\bar{L}-\varphi)$. Of course, if we have a localized structure $u(x)$ of length $2\bar{L}$ for some μ, we will also have a localized structure $u(-x)$ with length $2\bar{L}$ at this μ, so that in a bifurcation diagram plotting solution length or norm vs. μ, every point along a branch of asymmetric solutions will correspond to two separate asymmetric solutions related by $x \mapsto -x$. This can also be understood by noting that if $u(x)$ has phase φ, $u(-x)$ will have phase $\tilde{\varphi} = 2\pi - \varphi$, so that by virtue of the 2π-periodicity of z, $\mu = z(\bar{L}+\tilde{\varphi}) = z(\bar{L}-\tilde{\varphi})$ will be satisfied.

In summary, all solution branches can be found by determining the values of L and φ such that

$$Z(L,\varphi) := z(L+\varphi) - z(L-\varphi) = 0. \tag{3.1}$$

The corresponding values of μ for which these solutions exist are determined by the relation $\mu = z(L+\varphi)$, which is of course equivalent to $\mu = z(L-\varphi)$ for all (L,φ) such that $Z(L,\varphi) = 0$. In particular, since z is 2π-periodic, we will have symmetric localized solutions for any L with $\varphi = 0$ or $\varphi = \pi$, whereas asymmetric solutions will exist for particular values of L and $\varphi \notin \{0,\pi\}$ satisfying $Z(L,\varphi) = 0$. The resulting bifurcation diagram of symmetric and asymmetric branches, for z as given in Figure 7(i), is therefore as shown in Figure 1: to understand the shape of the bifurcation branches, we needed only the existence of fronts, $x \mapsto -x$ symmetry, and a relationship between the length of the interface region of fronts and a system parameter.

We now connect the function z and the bifurcation equation (3.1), obtained here via formal gluing arguments, to the rigorous results established in [3]. In that paper, it was shown that symmetric and asymmetric branches correspond to solutions of a system of the form

$$Z(L,\varphi) + \mathrm{O}(e^{-KL}) = 0 \tag{3.2}$$

for some constant $K > 0$: in particular, for L large enough, regular zeros of (3.1) correspond to regular zeros of (3.2), and vice versa. In particular, under hypotheses detailed in [3], $\mathcal{R}$-symmetric solutions that spend time $2L$ near the periodic orbit exist for points (μ, L) with $\mu = \mu_*(L,\varphi_0) = z(L+\varphi_0) + \mathrm{O}(e^{-KL})$ for some $K > 0$ with $\varphi_0 \in \{0,\pi\}$. Furthermore, all other single-pulse solutions that spend time $2L$ near the periodic orbit are exponentially close in L to the set of points (μ, L) such that $\mu = z(L+\varphi) = z(L-\varphi)$. Finally, it was shown in [3] that the function z appearing in (3.2) has a natural interpretation in terms of the intersection of invariant manifolds.

3.5 Bifurcation structure of localized solutions assuming $x \mapsto -x$ and $u \mapsto -u$ symmetry

In the presence of a $\mathbb{Z}_2$ symmetry κ, the main distinction from the above is that the function z is now automatically π-periodic: supposing our symmetry to be $u \mapsto -u$, if a front $u(x)$ of length l exists at some parameter value μ, then a front $-u(x)$ with characteristic length $(l+\pi)$ mod 2π must also exist at this μ; see Figure 9.

Thus $z(l) = z(l+\pi)$ for all l, i.e., z is π-periodic. As a consequence, the bifurcation branch of symmetric solutions with maxima in the center will lie on top of those with minima in the center [$z(L) = z(L+\pi)$.] Moreover, the branches of $\kappa\mathcal{R}$-symmetric solutions with $\varphi = \frac{\pi}{2}$ or $\varphi = \frac{3\pi}{2}$ described previously will lie on top of each other for the same reason. Of course, the branches of the $\mathcal{R}$- and $\kappa\mathcal{R}$-symmetric solutions will be offset from each other by half a period, so that they have the appearance of being intertwined.

Asymmetric solutions of length $2\bar{L}$ will again exist whenever we can satisfy $\mu = z(\bar{L}+\varphi) = z(\bar{L}-\varphi)$, keeping in mind that z is now π-periodic. Note that each point on a bifurcation branch of asymmetric solutions will now correspond to four such solutions: the "original" $u(x)$ plus $u(-x)$, $-u(x)$ and $-u(-x)$. We note in passing that all of these will satisfy $\mu = z(\bar{L}+\varphi) = z(\bar{L}-\varphi)$ for their particular φ, and that we will have exactly one solution with phase φ in each of the regions $(0,\frac{\pi}{2}), (\frac{\pi}{2},\pi), (\pi,\frac{3\pi}{2}), (\frac{3\pi}{2},2\pi)$.

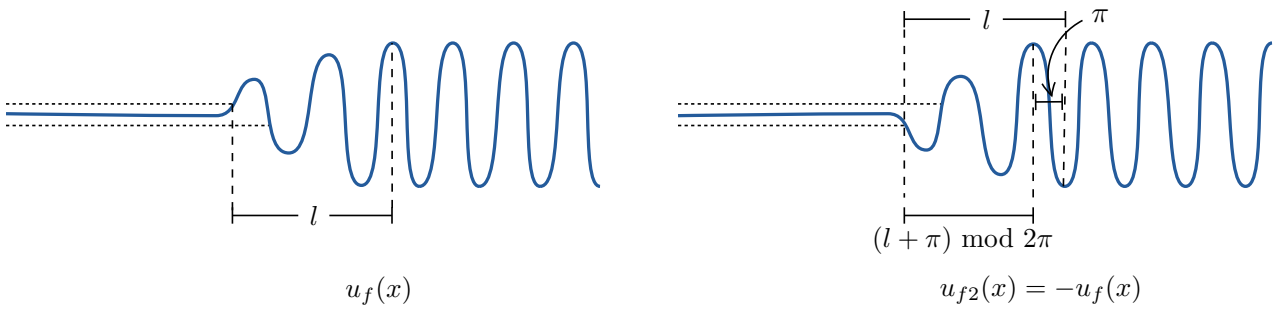

Figure 9: *Illustration that the function z will be π-periodic whenever the periodic orbit $v(x)$ respects both $x \mapsto -x$ and $u \mapsto -u$ symmetries.* Left: *A front $u_f(x)$ with characteristic length l, which we assume exists at some μ_0.* Right: *The front $u_{f2}(x) := -u_f(x)$ will also exist for this μ_0, and will have characteristic length $l + \pi$.*

Thus, as in the case where we had only $x \mapsto -x$ symmetry, we again see that the zero-level set of the function $Z(L, \varphi) := z(L + \varphi) - z(L - \varphi)$ describes all bifurcation branches of localized oscillatory structures. The $\mathcal{R}$-symmetric solution branches are those with $\varphi = 0$ and $\varphi = \pi$, while the $\kappa\mathcal{R}$ branches correspond to $\varphi = \frac{\pi}{2}$ and $\varphi = \frac{3\pi}{2}$. Both these solution types exist for all values of L. Finally, asymmetric solutions exist only for those values of L and $\varphi \notin \{0, \frac{\pi}{2}, \pi, \frac{3\pi}{2}\}$ such that $Z(L, \varphi) = 0$. See Figure 1 for the bifurcation diagram when z has the shape outlined in Figure 7(i).

Similar to the case without symmetry, these results have been derived rigorously in [3]: if a $\mathbb{Z}_2$ symmetry κ is present, the function z will be π rather than 2π-periodic, and two additional snaking branches with $\kappa\mathcal{R}$ symmetry will exist for $\mu = \mu_*(L, \varphi_0) = z(L + \varphi_0) + \mathrm{O}(e^{-KL})$ for some $K > 0$ with $\varphi_0 \in \{\frac{\pi}{2}, \frac{3\pi}{2}\}$.

4 Main results and predictions

Our goal now is to start with a system that respects the $\mathbb{Z}_2$ symmetry κ for all μ, and to describe what happens under forced symmetry breaking. To illustrate our approach, we start with the case where $z(L)$ possesses one maximum and one minimum for each period π, where the π-periodicity is enforced by the presence of a $\mathbb{Z}_2$ symmetry κ. We will be interested in perturbative terms breaking the κ symmetry when a second parameter ε is switched on, i.e., when $\varepsilon \neq 0$.

In Figure 10(a) we provide two equivalent renderings of the solution branches of localized structures in a system possessing κ symmetry and with $z(L)$ having a single maximum per period. We illustrate the branches of even and odd symmetric structures ($\mathcal{R}$- and $\kappa\mathcal{R}$-symmetric, respectively) as well as the asymmetric solution branches. The left panel shows the phase φ along the x-axis, and the half-pulse length L along the y-axis, while the center panel shows the solutions in the (μ, L) plane via the function $\mu = z(L + \varphi)$ for solutions (L, φ) of

$$Z(L, \varphi) := z(L + \varphi) - z(L - \varphi) = 0.$$

This is analogous to our usual bifurcation diagram, with length L being equivalent to the L^2 norm. The formulation in the left panel will provide a natural way to understand the effects of symmetry breaking perturbations, while the center panel provides the link to familiar bifurcation diagrams. We see that, before perturbation, the $\mathcal{R}$-symmetric solutions at $\varphi = 0$ and $\varphi = \pi$ coincide in the (μ, L) plane, as do the $\kappa\mathcal{R}$-symmetric solutions at $\varphi = \frac{\pi}{2}$ and $\varphi = \frac{3\pi}{2}$ (latter not shown). We also note that, due to the π-periodicity of z, all information is actually contained in a single quadrant of the left panel, but we show the larger diagram here for easier comparison with the diagram after symmetry breaking.

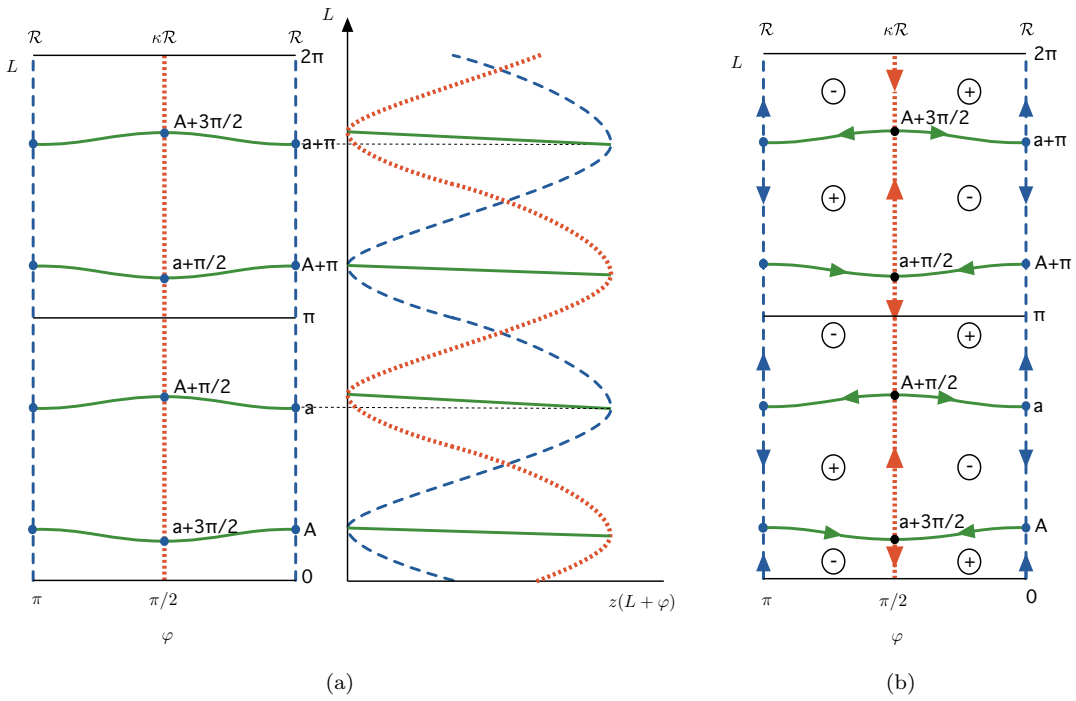

Figure 10: *We show different renderings of the bifurcation diagram for a system characterized by z possessing exactly one maximum and one minimum per period.* Left: *The solution set of the bifurcation equations $z(L-\varphi) = z(L+\varphi)$ is shown in the (φ, L)-plane.* Center: *The bifurcation diagram in the (μ, L)-plane, using the relation $\mu = z(L+\varphi)$. $\mathcal{R}$-symmetric solution branches with $\varphi = 0, \pi$ are shown in dashed blue, $\kappa\mathcal{R}$-symmetric with $\varphi = \frac{\pi}{2}, \frac{3\pi}{2}$ in dotted orange, and asymmetric in solid green. Light dotted lines indicate correspondence of a and $a+\pi$ with minima.* Right: *Reformulation of the left panel as a Hamiltonian system; see the text for full details.*

We now drop the assumption that z has only one maximum per period. We argued formally in Section 3 that it suffices to solve

$$Z(L,\varphi) := z(L+\varphi) - z(L-\varphi) = 0 \tag{4.1}$$

for (L, φ) in order to find symmetric and asymmetric solution branches. Indeed, it was shown in [3] that the bifurcation equations for symmetric and asymmetric solutions are given by (4.1) with an additional error term of order $\mathrm{O}(e^{-KL})$ for some $K > 0$: in particular, regular zeros of (4.1) persist as solutions to the full bifurcation equations for all sufficiently large L. The analysis in [3] applies to reversible PDEs with or without variational structure on cylinders provided the spatial dynamical system associated with the steady-state equation falls under the class considered in [19].

Our goal here is to study the effect of perturbative terms breaking the κ symmetry. It will be useful to consider the system presented in the left panel of Figure 10(a) as a dynamical system in its own right, a technique employed in [3]. We let $\bar{S}^1 := [0,\pi]/\sim$, set $Q := \bar{S}^1 \times [0, \frac{\pi}{2}]$, and define

$$\Lambda := \{(L,\varphi) \in Q : Z(L,\varphi) = 0\}, \quad \Lambda_{bif} := \{(L,\varphi) \in \partial Q : z'(L+\varphi) = 0\}.$$

We introduce the planar Hamiltonian vector field

$$\begin{pmatrix} L_s \\ \varphi_s \end{pmatrix} = F(L,\varphi) := \begin{pmatrix} 0 & 1 \\ -1 & 0 \end{pmatrix} \nabla Z(L,\varphi) \tag{4.2}$$

whose zero energy level is precisely equal to the set Λ. We note that

$$\nabla Z(L,\varphi) = \begin{pmatrix} 1 & -1 \\ 1 & 1 \end{pmatrix} \begin{pmatrix} z'(L+\varphi) \\ z'(L-\varphi) \end{pmatrix}.$$

Hence we have $\nabla Z(L,\varphi)=0$ if and only if $z'(L+\varphi)=z'(L-\varphi)=0$. Assuming nondegeneracy of the maxima and minima of z, i.e., assuming $z(L_1)=z(L_2)$ and $z'(L_1)=z'(L_2)=0$ imply $L_1=L_2 \bmod \pi$, we conclude that $\nabla Z(L,\varphi)=0$ for $(L,\varphi)\in\Lambda$ if and only if $\varphi\in\{0,\frac{\pi}{2}\}$. Thus all equilibria of (4.2) in Λ lie in Λ_{bif}. Furthermore, assuming $z'(L)=0$ implies $z''(L)\neq 0$, all equilibria in Λ are hyperbolic saddles, since at these points we have

$$DF(L,\varphi_0)=2\begin{pmatrix} z''(L+\varphi_0) & 0 \\ 0 & -z''(L+\varphi_0)\end{pmatrix},\quad \varphi_0\in\left\{0,\frac{\pi}{2}\right\}.$$

So by Poincarè-Bendixon, $\Lambda\backslash\Lambda_{bif}$ must be a 1D manifold consisting of the heteroclinic orbits that start and end at Λ_{bif}, and finitely many periodic orbits. Thus each element $(L_*,0)$ and $(L_*,\frac{\pi}{2})$ of Λ_{bif} is a generic pitchfork bifurcation point, which gives rise to a unique global branch of solutions of (4.1) in Q. These branches do not cross, and they begin and end in Λ_{bif}. In Figure 10(b) we reproduce the left panel of Figure 10(a) with arrows indicating the flow of (4.2) within the zero energy level set Λ of the Hamiltonian system just described, as well as plus and minus signs indicating the sign of the energy $Z(L,\varphi)$.

We are now ready to consider a perturbation which breaks the κ symmetry, but preserves the other characteristics of our system, meaning in particular that the reversibility is unaffected so that we retain the 2π-periodicity of z. Such a symmetry breaking perturbation will, however, typically break the π-periodicity of z and therefore break up the $\kappa\mathcal{R}$-symmetric branch. On the level of the vector field interpretation, this manifests itself as the fact that the saddle equilibria persist, but generically move outside the zero-level set of Z.

Lemma 4.1 *Suppose $z(L)$ is π-periodic, satisfying (a) $z(L_1)=z(L_2)$ and $z'(L_1)=z'(L_2)$ only if $L_1=L_2$ mod π and (b) $z'(L)=0$ implies $z''(L)\neq 0$. Let (L_0,φ_0) be a hyperbolic equilibrium of (4.2) satisfying (4.1). Assume $\tilde z(L,\varepsilon):=z(L)+\varepsilon z_1(L)+\mathrm{O}(\varepsilon^2)$, with $\tilde z(L,\varepsilon)$, and therefore $z_1(L)$, 2π-periodic in L. Further define $\tilde Z(L,\varphi,\varepsilon):=\tilde z(L+\varphi,\varepsilon)-\tilde z(L-\varphi,\varepsilon)$, and consider*

$$\begin{pmatrix} L_s \\ \varphi_s\end{pmatrix}=\tilde F(L,\varphi,\varepsilon):=\begin{pmatrix} 0 & 1 \\ -1 & 0\end{pmatrix}\nabla\tilde Z(L,\varphi,\varepsilon). \tag{4.3}$$

Then there exists an $\varepsilon_0>0$ such that the following hold:

(i) If $\varphi_0\in\{0,\pi\}$, then for all $|\varepsilon|<\varepsilon_0$ there exists a unique $\tilde L_0(\varepsilon)$ close to L_0 such that $(\tilde L_0(\varepsilon),\varphi_0,\varepsilon)$ is a hyperbolic equilibrium of (4.3), and $\tilde Z(\tilde L_0(\varepsilon),\varphi_0,\varepsilon)=0$. Furthermore, the function $\varepsilon\mapsto\tilde L_0(\varepsilon)$ is smooth.

(ii) If $\varphi_0\in\{\frac{\pi}{2},\frac{3\pi}{2}\}$, then for all $|\varepsilon|<\varepsilon_0$ there exists a unique $(\tilde L_0,\tilde\varphi_0)(\varepsilon)$ close to (L_0,φ_0) such that $((\tilde L_0,\tilde\varphi_0)(\varepsilon),\varepsilon)$ is a hyperbolic equilibrium of (4.3). Furthermore, the function $\varepsilon\mapsto(\tilde L_0,\tilde\varphi_0)(\varepsilon)$ is smooth, and if $z_1(L_0+\varphi_0)\neq z_1(L_0-\varphi_0)$, then $\tilde Z((\tilde L_0,\tilde\varphi_0)(\varepsilon),\varepsilon)\neq 0$.

Proof. Given $\tilde F$ as defined in (4.3), we can write $\tilde F$ explicitly as

$$\tilde F(L,\varphi,\varepsilon)=\begin{pmatrix}\tilde z(L+\varphi,\varepsilon)+\tilde z(L-\varphi,\varepsilon)\\ -\tilde z(L+\varphi,\varepsilon)+\tilde z(L-\varphi,\varepsilon)\end{pmatrix}=\begin{pmatrix} z'(L+\varphi)+\varepsilon z_1'(L+\varphi)+z'(L-\varphi)+\varepsilon z_1'(L-\varphi)+\mathrm{O}(\varepsilon^2)\\ -z'(L+\varphi)-\varepsilon z_1'(L+\varphi)+z'(L-\varphi)+\varepsilon z_1'(L-\varphi)+\mathrm{O}(\varepsilon^2)\end{pmatrix}.$$

Whether we are in case (i) where $\varphi_0\in\{0,\pi\}$, or case (ii) where $\varphi_0\in\{\frac{\pi}{2},\frac{3\pi}{2}\}$, the π-periodicity of z implies $z''(L_0+\varphi_0)=z''(L_0-\varphi_0)$ so that

$$D\tilde F(L_0,\varphi_0,0)=\begin{pmatrix} 2z''(L+\varphi_0) & 0 & z_1'(L_0+\varphi_0)+z_1'(L_0-\varphi_0)\\ 0 & -2z''(L_0+\varphi_0) & -z_1'(L_0+\varphi_0)+z_1'(L_0-\varphi_0)\end{pmatrix}. \tag{4.4}$$

Since we have assumed $z''(L_0+\varphi_0)\neq 0$, this implies that there exists a $\varepsilon_0>0$ such that for all $|\varepsilon|<\varepsilon_0$, there exists a unique $(\tilde L_0,\tilde\varphi_0)(\varepsilon)$ close to (L_0,φ_0) such that $((\tilde L_0,\tilde\varphi_0)(\varepsilon),\varepsilon)$ is a hyperbolic equilibrium of (4.3), and the map $\varepsilon\mapsto(\tilde L_0,\tilde\varphi_0)(\varepsilon)$ is smooth.

In particular, we can solve for $(\tilde{L}_0, \tilde{\varphi}_0)(\varepsilon)$ as:

$$\tilde{F}(L, \varphi, \varepsilon) = \tilde{F}(L_0, \varphi_0, 0) + D\tilde{F}(L_0, \varphi_0, 0) \begin{pmatrix} L - L_0 \\ \varphi - \varphi_0 \\ \varepsilon \end{pmatrix} + \mathrm{O}(\varepsilon^2) = \begin{pmatrix} 0 \\ 0 \end{pmatrix}$$

so

$$\begin{pmatrix} 2z''(L_0 + \varphi_0)(L - L_0) + (z_1'(L_0 + \varphi_0) + z_1'(L_0 - \varphi_0))\varepsilon \\ -2z''(L_0 + \varphi_0)(\varphi - \varphi_0) + (-z_1'(L_0 + \varphi_0) + z_1'(L_0 - \varphi_0))\varepsilon \end{pmatrix} + \mathrm{O}(\varepsilon^2) = \begin{pmatrix} 0 \\ 0 \end{pmatrix}$$

yielding

$$L - L_0 = \varepsilon \left(\frac{-z_1'(L_0 + \varphi_0) - z_1'(L_0 - \varphi_0)}{2z''(L_0 + \varphi_0))} \right) + \mathrm{O}(\varepsilon^2)$$

$$\varphi - \varphi_0 = \varepsilon \left(\frac{-z_1'(L_0 + \varphi_0) + z_1'(L_0 - \varphi_0)}{2z''(L_0 + \varphi_0))} \right) + \mathrm{O}(\varepsilon^2)$$

or

$$(\tilde{L}_0, \tilde{\varphi}_0)(\varepsilon) = (L_0, \varphi_0) + \frac{\varepsilon}{2z''(L_0 + \varphi_0)} \left(-z_1'(L_0 + \varphi_0) - z_1'(L_0 - \varphi_0), -z_1'(L_0 + \varphi_0) + z_1'(L_0 - \varphi_0) \right) + \mathrm{O}(\varepsilon^2).$$

In case (i) where $\varphi_0 \in \{0, \pi\}$, the 2π-periodicity of $z_1(L)$ yields

$$(\tilde{L}_0, \tilde{\varphi}_0)(\varepsilon) = (L_0, \varphi_0) + \frac{\varepsilon}{2z''(L_0 + \varphi_0)} \left(-2z_1'(L_0 + \varphi_0), 0 \right) + \mathrm{O}(\varepsilon^2).$$

In fact, for $\varphi_0 \in \{0, \pi\}$, the 2π-periodicity of $\tilde{z}(L, \varepsilon)$ in L implies that

$$\tilde{F}(L, \varphi_0, \varepsilon) = 2 \begin{pmatrix} \tilde{z}'(L + \varphi_0) \\ 0 \end{pmatrix}.$$

So the unique $(\tilde{L}_0, \tilde{\varphi}_0)(\varepsilon)$ near (L_0, φ_0) satisfying $\tilde{F}((\tilde{L}_0, \tilde{\varphi}_0)(\varepsilon), \varepsilon) = 0$ must be of the form $(\tilde{L}_0(\varepsilon), \varphi_0)$ where $\tilde{L}_0(\varepsilon)$ satisfies $z'(\tilde{L}_0(\varepsilon) + \varphi_0) + \varepsilon z_1'(\tilde{L}_0(\varepsilon) + \varphi_0) = 0$.

This then implies

$$\tilde{Z}(\tilde{L}_0(\varepsilon), \varphi_0, \varepsilon) = z(\tilde{L}_0(\varepsilon) + \varphi_0) + \varepsilon z_1(\tilde{L}_0(\varepsilon) + \varphi_0) - z(\tilde{L}_0(\varepsilon) - \varphi_0) + \varepsilon z_1(\tilde{L}_0(\varepsilon) - \varphi_0) = 0$$

as $\tilde{z}$ is 2π-periodic. Thus we have shown (i).

In case (ii) where $\varphi_0 \in \{\frac{\pi}{2}, \frac{3\pi}{2}\}$ we have

$$\begin{aligned} \tilde{Z}((\tilde{L}_0, \tilde{\varphi}_0)(\varepsilon), \varepsilon) = {} & z \left(L_0 + \varphi_0 - \frac{\varepsilon z_1'(L_0 + \varphi_0)}{z''(L_0 + \varphi_0)} \right) + \varepsilon z_1 \left(L_0 + \varphi_0 - \frac{\varepsilon z_1'(L_0 + \varphi_0)}{z''(L_0 + \varphi_0)} \right) \\ & - z \left(L_0 - \varphi_0 - \frac{\varepsilon z_1'(L_0 - \varphi_0)}{z''(L_0 + \varphi_0)} \right) - \varepsilon z_1 \left(L_0 - \varphi_0 - \frac{\varepsilon z_1'(L_0 - \varphi_0)}{z''(L_0 + \varphi_0)} \right) + \mathrm{O}(\varepsilon^2). \end{aligned} \quad (4.5)$$

We expand

$$z \left(L_0 + \varphi_0 - \frac{\varepsilon z_1'(L_0 + \varphi_0)}{z''(L_0 + \varphi_0)} \right) = z(L_0 + \varphi_0) + 2z'(L_0 + \varphi_0) \left(\frac{-\varepsilon z_1'(L_0 + \varphi_0)}{z''(L_0 + \varphi_0)} \right) + \mathrm{O}(\varepsilon^2)$$

and similarly for $z \left(L_0 - \varphi_0 - \frac{\varepsilon z_1'(L_0 - \varphi_0)}{z''(L_0 + \varphi_0)} \right)$.

We also recall that $z'(L_0 + \varphi_0) = z'(L_0 - \varphi_0) = 0$, and $z(L_0 + \varphi_0) - z(L_0 - \varphi_0) = 0$. Thus we rewrite (4.5) as

$$\tilde{Z}((\tilde{L}_0, \tilde{\varphi}_0)(\varepsilon), \varepsilon) = \varepsilon z_1(L_0 + \varphi_0) - \varepsilon z_1(L_0 - \varphi_0) + \mathrm{O}(\varepsilon^2)$$

so that $\tilde{Z}((\tilde{L}_0, \tilde{\varphi}_0)(\varepsilon), \varepsilon) \neq 0$ as long as $z_1(L_0 + \varphi_0) \neq z_1(L_0 - \varphi_0)$. This completes the proof of (ii). ∎

The key point of the above is that saddle equilibria corresponding to pitchfork bifurcations from the $\kappa\mathcal{R}$-symmetric branches generically do not remain in the zero-level set of Z once the κ symmetry is broken, so that the $\kappa\mathcal{R}$-symmetric branches are themselves broken in a manner consistent with the Hamiltonian vector field formulation described above.

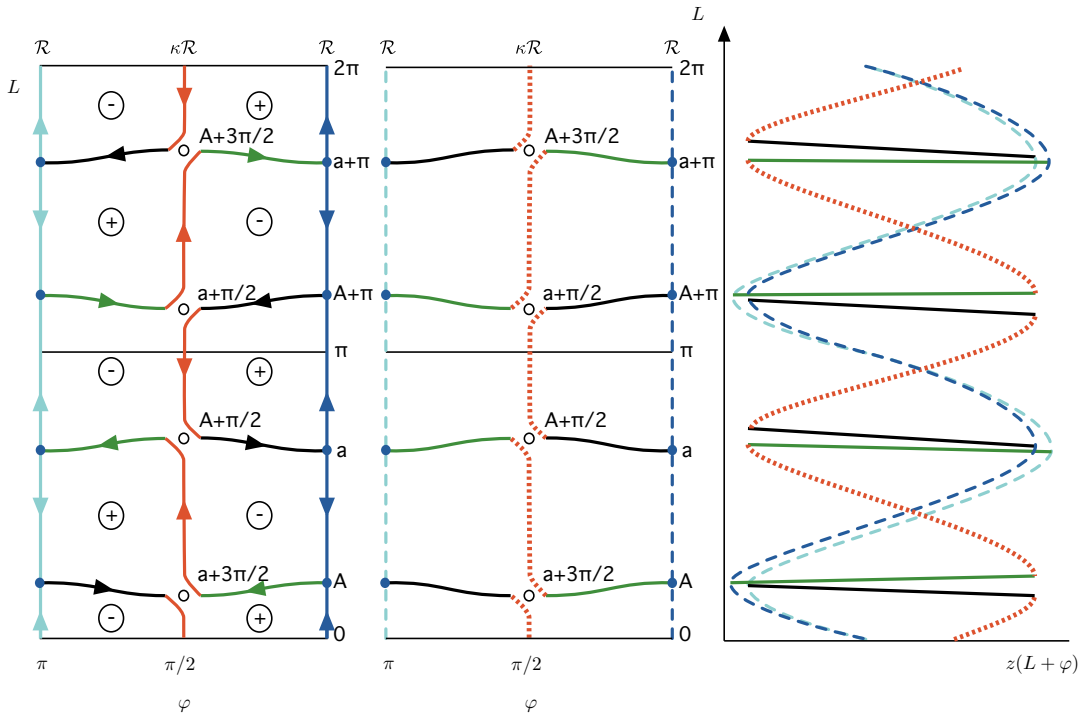

Figure 11: *Bifurcation diagram for a system as in Figure 10(a) after κ symmetry breaking. On the left is the interpretation of the branches as zero energy solutions of a Hamiltonian system, as in Figure 10(b); in the center is the same diagram without the vector field interpretation; and on the right the branches are shown in the $(\mu = z(L+\varphi), L)$ plane. The $\mathcal{R}$-symmetric branches, now appearing as two branches in the right-hand figure are shown in dashed dark and light blue for $\varphi = 0$ and π, respectively. The remains of the $\kappa\mathcal{R}$ symmetric branch, which now form sections of asymmetric branches, are shown in dotted orange. The portions of the asymmetric solution branches that were already asymmetric branches in the unperturbed case are shown in solid green and solid black to facilitate comparison of the diagrams.*

4.1 Systems such that z has a single maximum per period

Returning to the case where z has only one maximum and minimum per period, in Figure 11 we illustrate one possible result of κ symmetry breaking in such a system. In particular, using notation from the figure and Lemma 4.1, we have illustrated the case where $z_1(A) > z_1(A+\pi)$ and $z_1(a) > z_1(a+\pi)$. This means that the saddle equilibrium near $(A+\frac{\pi}{2}, \frac{\pi}{2})$ will now lie in the region where $\tilde{Z} < 0$, since

$$z_1\left(\left(A+\frac{\pi}{2}\right)+\frac{\pi}{2}\right) = z_1(A+\pi) < z_1(A) = z_1\left(\left(A+\frac{\pi}{2}\right)-\frac{\pi}{2}\right).$$

Similarly, the equilibrium near $(a-\frac{\pi}{2}, \frac{\pi}{2})$ will lie in the region where $\tilde{Z} > 0$, since

$$z_1\left(\left(a-\frac{\pi}{2}\right)+\frac{\pi}{2}\right) = z_1(a) > z_1(a+\pi) = z_1(a-\pi) = z_1\left(\left(a-\frac{\pi}{2}\right)-\frac{\pi}{2}\right).$$

Note that the 2π-periodicity of z_1 implies that the sign of $\tilde{Z}$ for the saddle equilibria with $L \in [0,\pi)$ fixes the sign of $\tilde{Z}$ for the saddle equilibria with $L \in [\pi, 2\pi)$; specifically, the sign will be opposite.

Technically there are four possible generic bifurcation diagrams, one for each of the four possible combinations of the sign of $\tilde{Z}$ at saddle equilibria near $(A+\frac{\pi}{2}, \frac{\pi}{2})$ and $(a-\frac{\pi}{2}, \frac{\pi}{2})$. However, as is clear from the preceding discussion, the sign combinations $(+,+)$ and $(-,-)$ are equivalent under translation by π in L, which amounts to swapping our definition of the $\varphi = 0$ and $\varphi = \pi$ branches. This equivalence also holds for the sign combinations $(+,-)$ and $(-,+)$. Furthermore, these two sets of "same sign" and "opposite sign" bifurcation diagrams are

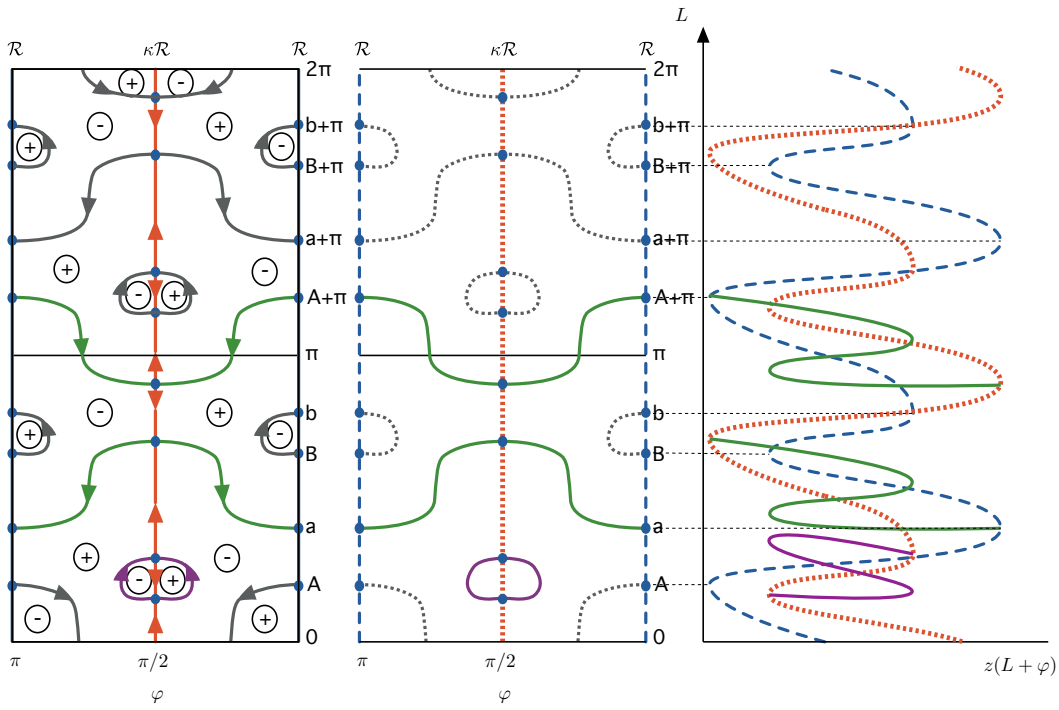

Figure 12: *Bifurcation structure of a system characterized by π-periodic z possessing two distinct maxima per period. Again, we illustrate the solution branches in the (φ, L) plane, both with and without the vector field interpretation, as well as in the $(\mu = z(L+\varphi), L)$ plane, where the actual bifurcation branches will be exponentially close in L to the ones shown. As before, $\mathcal{R}$-symmetric solution branches are shown in dashed blue, and $\kappa\mathcal{R}$-symmetric in dotted orange. Particular asymmetric solution branches are shown in solid purple and green. For clarity, not all asymmetric solution branches are shown in the right-most rendering; branches not shown on the right are rendered in thin dotted gray in the center illustration. The light dashed horizontal lines show the correspondence between the hyperbolic equilibria at A, a, B, b, etc. and the maxima and minima on the right.*

in fact qualitatively equivalent as both result in a series of alternating cross-connecting and self-connecting asymmetric branches, each with two saddle nodes. In terms of the familiar bifurcation diagram in the (μ, L) plane, self-connecting branches will appear as 'S' shaped curves and cross-connecting as 'Z' shaped curves for perturbations such that the sign of $\tilde{Z}$ is the same $[(+,+)$ or $(-,-)]$ for saddle equilibria with $L \in [0, \pi)$ near $\varphi = \pi/2$. The opposite is true for perturbations such that the sign of $\tilde{Z}$ is $(+,-)$ or $(-,+)$. As we will see below, when z has two or more maxima, different symmetry breaking perturbations may result in distinct bifurcation diagrams, which are not reducible via reflections or translations.

We note that these results are applicable to localized roll solutions of the one-dimensional Swift–Hohenberg model

$$u_t = -(1 + \partial_x^2)^2 u - \mu u + \nu u^3 - u^5, \quad x \in \mathbb{R} \tag{4.6}$$

with the addition of perturbative terms, regardless of whether these terms preserve the variational structure. Indeed, we observe that these findings are entirely consistent with the numerical results of Houghton and Knobloch, including the breaking up of the odd parity branches, broadening of the snaking region, and appearance of S and Z asymmetric branches.

4.2 Systems such that z has at least two maxima per period

We now turn to the somewhat more complicated situation where $z(L)$ possesses two maxima and minima per period π; of course the periodicity implies that maxima and minima must occur in pairs.

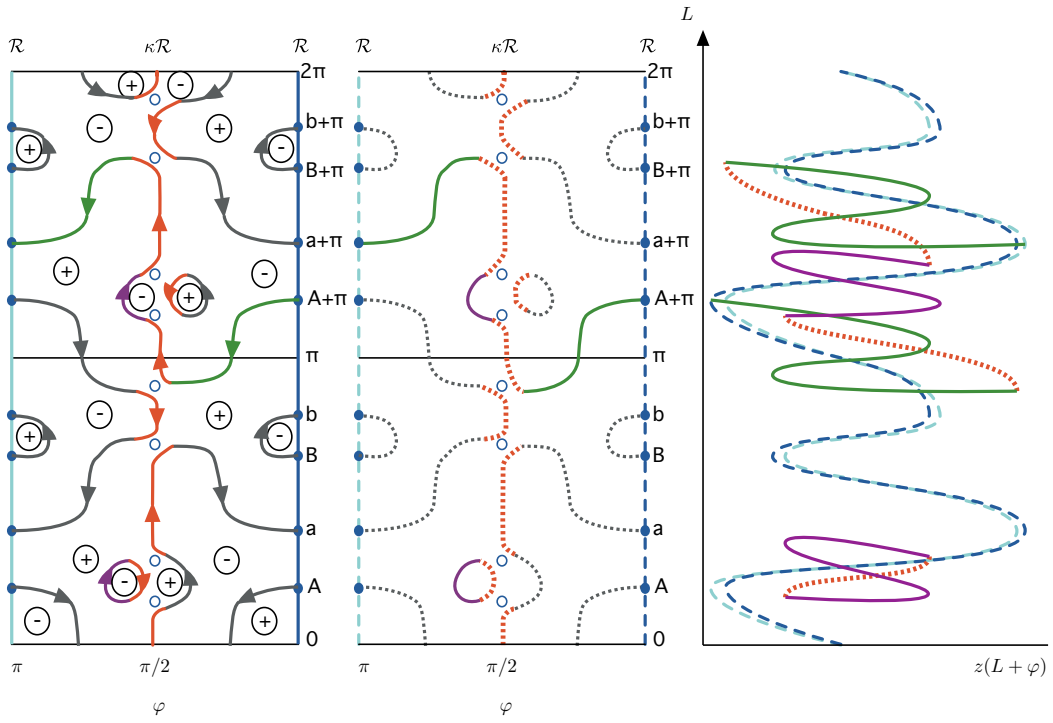

Figure 13: *Bifurcation structure of the system illustrated in Figure 12, after the addition of a κ symmetry breaking perturbative term causing the sign of Z to be the same at adjacent local extrema. Again for clarity, only a selection of asymmetric solution branches are shown in the right-most figure. The coloring and line styles from Figure 12 have been preserved to show the portions of each solution branch arising from the original branches in the unperturbed case. Note that although all branch segments bifurcating from the $\kappa\mathcal{R}$-symmetric branch remain dotted orange in the center figure, not all segments are shown on the right.*

Figure 12 shows a rendering of the resulting bifurcation structure for such a z. Again the left and center panels show the phase φ along the x-axis the pulse length L along the y-axis, while the right-hand figure shows the analogous plot to a typical bifurcation diagram. Once more, prior to perturbation, the $\mathcal{R}$-symmetric solutions at 0 and π coincide in the $(\mu = z(L+\varphi), L)$ plane, as do the $\kappa\mathcal{R}$-symmetric solutions at $\frac{\pi}{2}$ and $\frac{3\pi}{2}$. Again to enable later comparisons, we show the right and center diagrams for $(\varphi, L) \in [0,\pi] \times [0, 2\pi]$ even though all information is contained in the $[0, \frac{\pi}{2}] \times [0, \pi]$ quadrant.

We note that this form of z is observed for the planar stripe and spot patterns seen in the cubic-quintic Swift–Hohenberg posed on a cylinder, i.e.,

$$u_t = -(1 + \partial_x^2 + \partial_y^2)^2 u - \mu u + \nu u^3 - u^5, \quad (x, y) \in S^1 \times \mathbb{R} \tag{4.7}$$

where $S^1 = \mathbb{R}/2L_x\mathbb{Z}$ for some $L_x > 0$, and that the branches in Figure 12 are indeed consistent with the full bifurcation structure of the almost-planar stripe and spot patterns in the cubic-quintic Swift–Hohenberg model, as reported in [2] and also verified in Section 5 below.

Upon introduction of a perturbative term breaking the κ symmetry, we again expect that the $\kappa\mathcal{R}$-symmetric branches will break up, with the saddle equilibria generically moving outside the zero-level set of $\tilde{Z}$ due to the loss of π-periodicity of z, i.e., due to the fact that generically $z_1(L_0 + \varphi_0) \neq z_1(L_0 - \varphi_0)$. However, in contrast to the single maximum system discussed above, here we find that we obtain qualitatively different bifurcation diagrams depending on whether the new sign of $\tilde{Z}$ at adjacent saddle equilibria matches or differs.

In particular, there are now sixteen possible generic bifurcation diagrams, one for each of the possible combinations for the sign of $\tilde{Z}$ at saddle equilibria near $(B - \frac{\pi}{2}, \frac{\pi}{2})$, $(b - \frac{\pi}{2}, \frac{\pi}{2})$, $(A + \frac{\pi}{2}, \frac{\pi}{2})$ and $(a + \frac{\pi}{2}, \frac{\pi}{2})$, where the labels

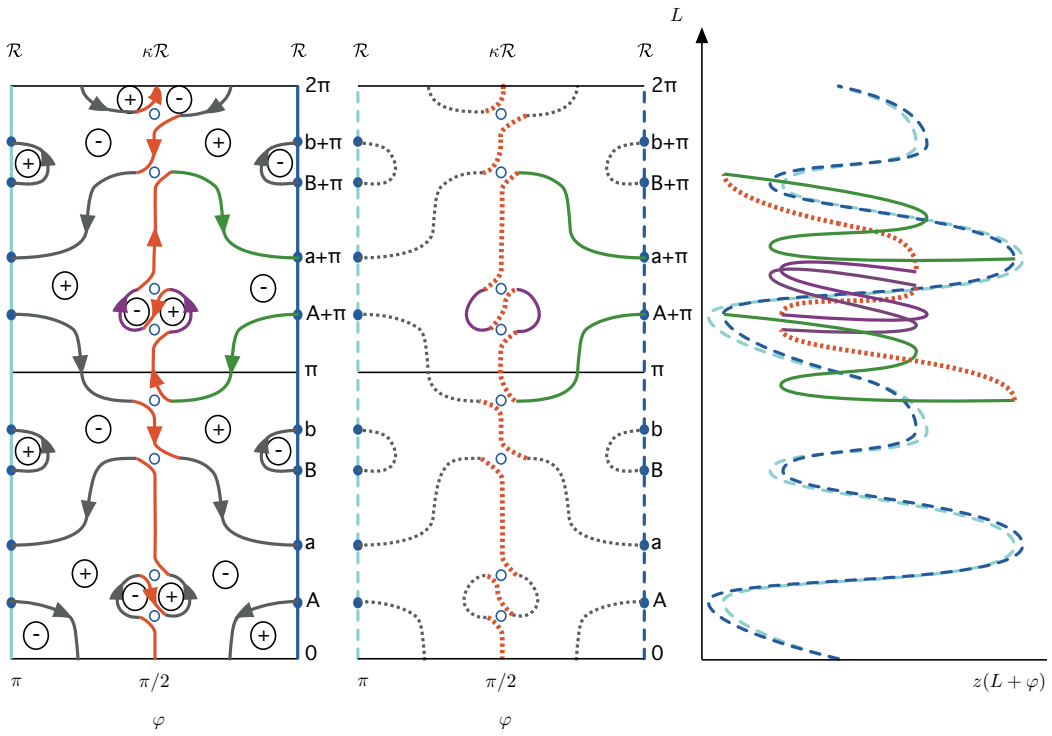

Figure 14: *Symmetry breaking with the opposite relative movement of adjacent local extrema from that displayed in Figure 13. Note that for clarity we no longer show a cross-connecting asymmetric solution, but focus instead on one of the self-connecting asymmetric branch with 14 saddle nodes.*

correspond to those used in Figure 12. Once again the 2π-periodicity of z_1 implies that the saddle equilibria with $L \in [\pi, 2\pi)$ will have $\tilde{Z}$ of the opposite sign as the corresponding saddle equilibria with $L \in [0, \pi)$.

Noting that B and b are local (rather than global) extrema of the function z, the biggest qualitative difference in possible bifurcation diagrams is between those in which the saddle equilibria near $(B - \frac{\pi}{2}, \frac{\pi}{2})$ and $(b - \frac{\pi}{2}, \frac{\pi}{2})$ have $\tilde{Z}$ with the same sign, versus those in which the sign of $\tilde{Z}$ is different. In the former case, the bifurcation diagram for the perturbed system will possess isolas formed from the reorganization of asymmetric and $\kappa\mathcal{R}$-symmetric branches, whereas in the latter the bifurcation diagram will have self-connecting asymmetric branches with many saddle nodes, but no isolas.

This distinction holds regardless of the sign of $\tilde{Z}$ at the remaining saddle equilibria, i.e., those corresponding to global maxima and minima. Differences in the sign of $\tilde{Z}$ for the saddle equilibria near $(A + \frac{\pi}{2}, \frac{\pi}{2})$ and $(a + \frac{\pi}{2}, \frac{\pi}{2})$ affect the number of saddle nodes in each asymmetric branch, but do not affect the formation of isolas. We note that, by inspection of the Hamiltonian vector field formulation, the exact number of saddle nodes on any given bifurcation branch can be determined by counting the number of tangencies to one of the vectors $(\pm 1, \pm 1)$ in the (φ, L) plane.

In Figure 13, we illustrate the form the bifurcation diagram should take under a perturbation such that z_1 at adjacent local extrema B and b satisfies $z_1(B) > z_1(B + \pi)$ and $z_1(b) > z_1(b + \pi)$. This means that the saddle equilibrium near $(B - \frac{\pi}{2}, \frac{\pi}{2})$ will now lie in the region where $\tilde{Z} > 0$, since

$$z_1\left(\left(B - \frac{\pi}{2}\right) + \frac{\pi}{2}\right) = z_1(B) > z_1(B + \pi) = z_1(B - \pi) = z_1\left(\left(B - \frac{\pi}{2}\right) - \frac{\pi}{2}\right).$$

The equilibrium near $(b - \frac{\pi}{2}, \frac{\pi}{2})$ will also lie in the region where $\tilde{Z} > 0$, since

$$z_1\left(\left(b - \frac{\pi}{2}\right) + \frac{\pi}{2}\right) = z_1(b) > z_1(b + \pi) = z_1(b - \pi) = z_1\left(\left(b - \frac{\pi}{2}\right) - \frac{\pi}{2}\right).$$

Again we observe that whether $z_1(B) > z_1(B+\pi)$ and $z_1(b) > z_1(b+\pi)$ or the opposite inequalities hold is immaterial as long as they are both in the same direction. Identifying these two cases amounts to reversing our conventions for defining $\varphi = 0$ and $\varphi = \pi$. In Section 5, we demonstrate the formation of isolas numerically for the Swift–Hohenberg model, with symmetry-breaking perturbation εu^2.

In contrast, in the case where the perturbation causes one local extremum to move up and the other to move down relative to those at distance π, we do not expect isolas, but rather anticipate a complicated asymmetric branch possessing 14 saddle nodes, as shown in Figure 14. In particular, we illustrate the case where $z_1(B) < z_1(B+\pi)$ and $z_1(b) > z_1(b+\pi)$, along with $z_1(A) > z_1(A+\pi)$ and $z_1(a) < z_1(a+\pi)$. As seen in Section 5, this type of behavior is observed in the Swift–Hohenberg model with the perturbative term εu^4.

This sort of analysis can be continued for z possessing more than two maxima per period. We reiterate that in order for symmetry breaking to produce isolas, a minimum of two maxima (and minima) are required prior to the introduction of symmetry breaking terms.

5 Numerical results and confirmation of predictions

5.1 Numerical verification of Section 4 predictions

We begin by confirming that the planar stripe and spot pattern of

$$u_t = -(1+\partial_x^2+\partial_y^2)^2 u - \mu u + \nu u^3 - u^5, \quad (x,y) \in S^1 \times \mathbb{R} \tag{5.1}$$

where $S^1 = \mathbb{R}/2L_x\mathbb{Z}$ for some $L_x > 0$, has the bifurcation structure diagrammed in Figure 12 of Section 4 above; we refer to [2] for the original computation.

All numerical simulations were completed in MATLAB, using a modified version of EPCONT, a predecessor of COCO [12], as in [2]. The modifications made to EPCONT include employing the Newton trust-region solver FSOLVE, and projecting out the approximate translation directions in each predictor step. We use spectral differentiation matrices in the periodic x-direction, and finite differences in the y-direction. In particular, all figures shown in this section were calculated via numerical continuation with $n_x = 8$ Fourier modes and $n_y = 800$ equidistant points on the domain $(0,\pi) \times (-50,50)$ with Neumann boundary conditions.

Figures 15(a) and 15(b) show the bifurcation diagram for the stripe and spot pattern of (5.1), along with selected solution profiles. In (a) we show an asymmetric solution along with two $\mathcal{R}$-symmetric solutions existing for the same μ, and similarly in (b) we show an asymmetric solution and two $\kappa\mathcal{R}$-symmetric solutions, where $\kappa : u(x) \mapsto -u(L_x - x)$. We note that both sets of solutions profiles are consistent with the gluing interpretation.

We next demonstrate a perturbation leading to the bifurcation structure predicted in Section 4, and diagrammed in Figure 13. Using the perturbative term εu^2, i.e.,

$$u_t = -(1+\Delta)^2 u - \mu u + \nu u^3 - u^5 + \varepsilon u^2 \tag{5.2}$$

we find that we do indeed observe the predicted isolas bifurcating where we expect them, as shown in Figure 16.

We can also calculate the distance from $\kappa\mathcal{R}$ symmetry for each solution lying along the branch; doing this for the isola, we note that the middle portion is indeed almost perfectly $\kappa\mathcal{R}$ symmetric, as expected; see Figure 18.

For completeness, in Figure 19 we also include the results of numerical continuation on the planar stripe and spot patterns with perturbative term εu^4, i.e.,

$$u_t = -(1+\Delta)^2 u - \mu u + \nu u^3 - u^5 + \varepsilon u^4 \tag{5.3}$$

We see that this type of perturbation causes adjacent saddle equilibria to move in opposite directions, or equivalently that one local extremum moves up while the other to moves down relative to the local extrema at distance π. Consequently this bifurcation diagram corresponds to the schematic displayed in Figure 14.

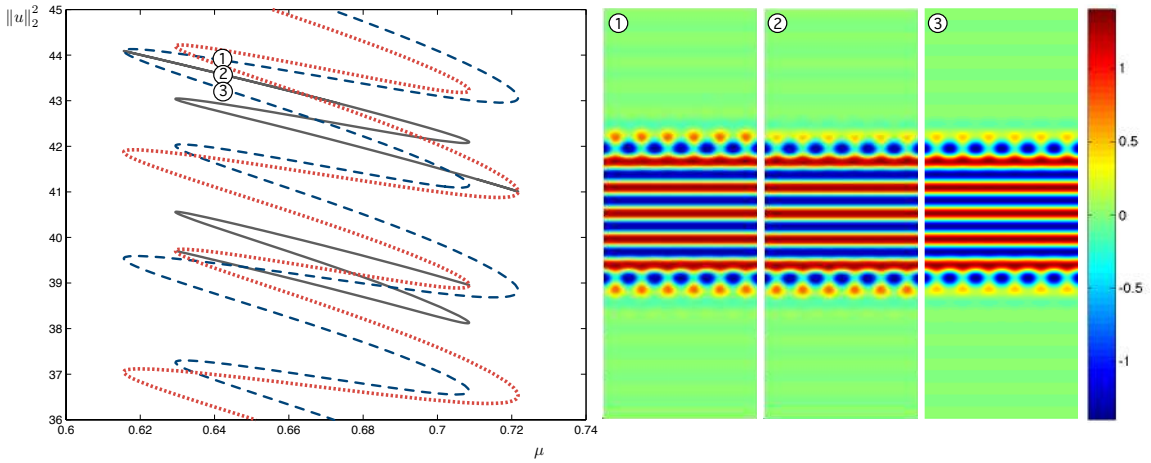

(a) Bifurcation diagram for planar stripes and spots, with numbers indicating the locations of two $\mathcal{R}$-symmetric solutions, and the intermediate cross-connecting asymmetric solution shown at right; see [2].

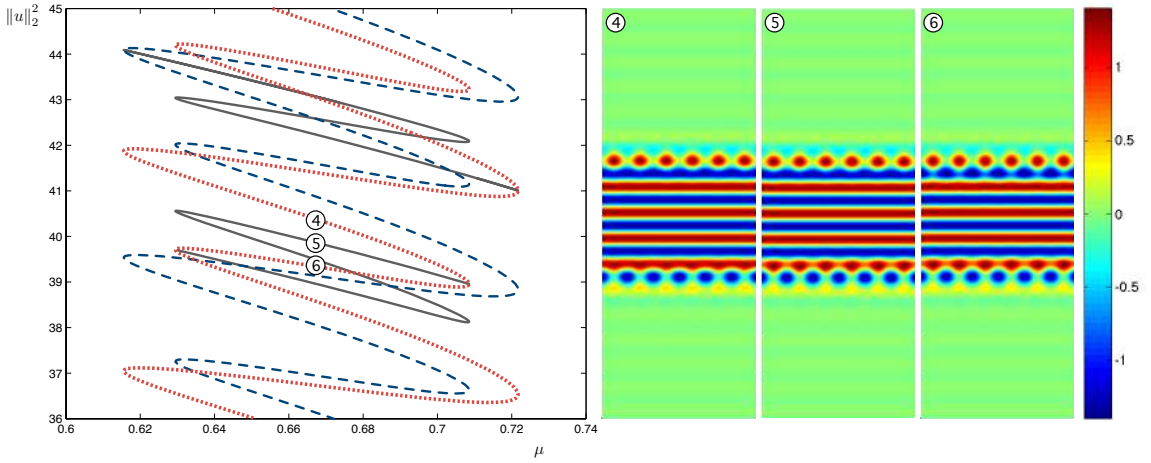

(b) Bifurcation diagram for planar stripes and spots, with numbers indicating the locations of the two $\kappa\mathcal{R}$-symmetric and the intermediate self-connecting asymmetric solution shown at right; see [2].

Figure 15: *Bifurcation diagram for planar stripes and spots in (5.1), along with locations of solution profiles shown at right. $\mathcal{R}$-symmetric branch shown in dashed blue, $\kappa\mathcal{R}$-symmetric branch in dotted orange, and representative asymmetric branches in solid gray. The colorbar is the same for all solution profiles, and recalling that solutions are periodic in the x-direction, we show 6 periods for each solution.*

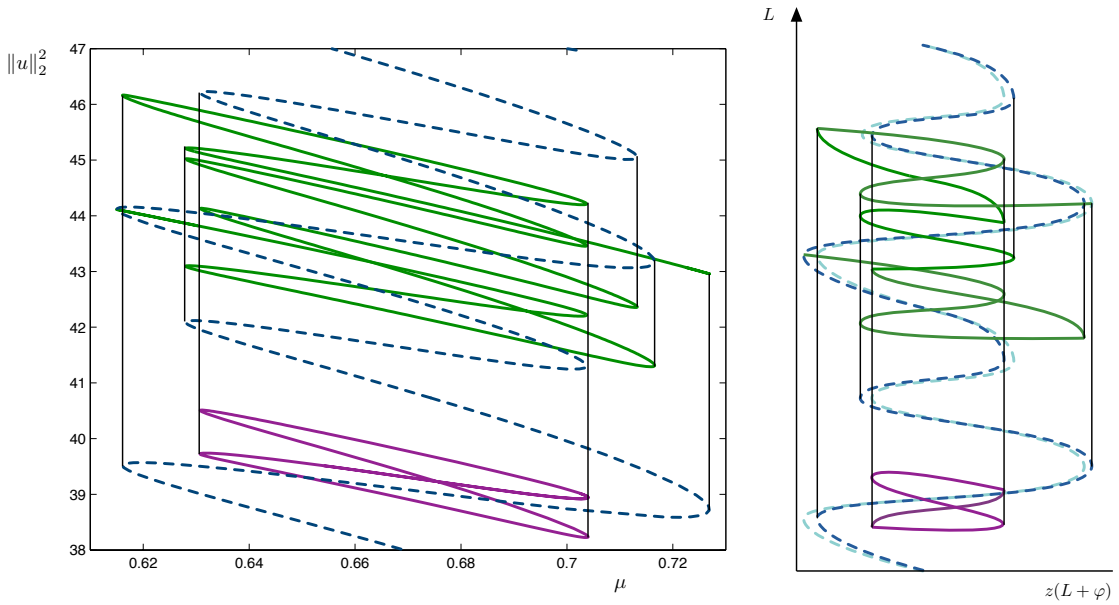

Figure 16: Left: *Partial bifurcation diagram for (5.2) with $\varepsilon = -0.01$, showing an isola in solid purple, along with one of two $\mathcal{R}$-symmetric branches with $\varepsilon = -0.01$ in dashed blue, and a cross-connecting asymmetric branch in solid green. Vertical lines indicate the correspondence between the extrema (saddle nodes) of the $\mathcal{R}$-symmetric branch and the saddle nodes of the asymmetric branches, including the isola. The cross-connecting asymmetric branch extends beyond the $\mathcal{R}$-symmetric branch as it terminates at the other $\mathcal{R}$-symmetric branch with phase $\varphi = \pi$ (not shown.)* Right: *Reproduction of the predicted bifurcation diagram from Figure 13, with vertical lines showing alignments of saddle nodes, as in the numerically computed bifurcation diagram.*

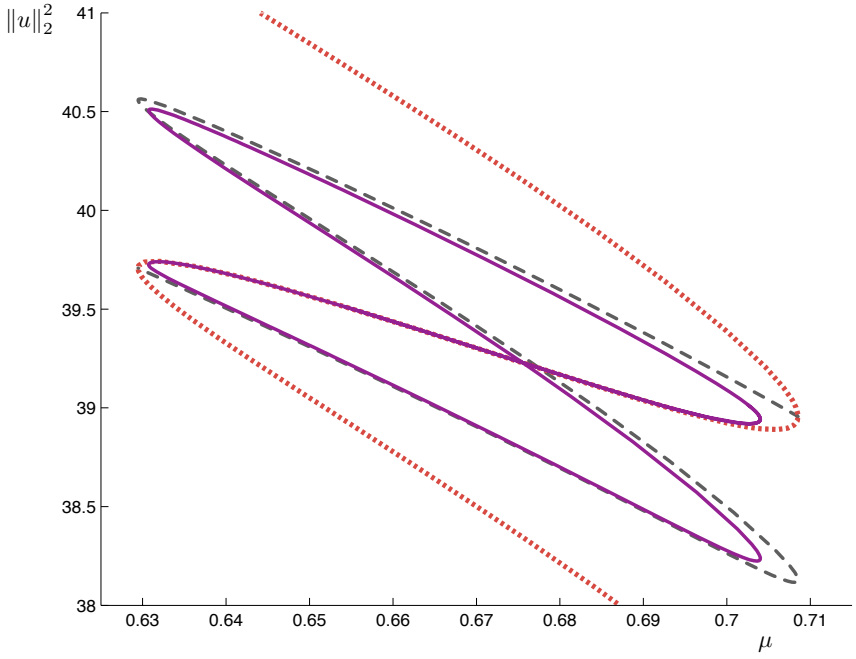

Figure 17: *For comparison purposes, the isola for (5.2) with $\varepsilon = -0.01$ is again shown in solid purple, along with the original ($\varepsilon = 0$) $\kappa\mathcal{R}$-symmetric branch in dotted orange, and the original ($\varepsilon = 0$) self-connecting asymmetric branch in dashed gray.*

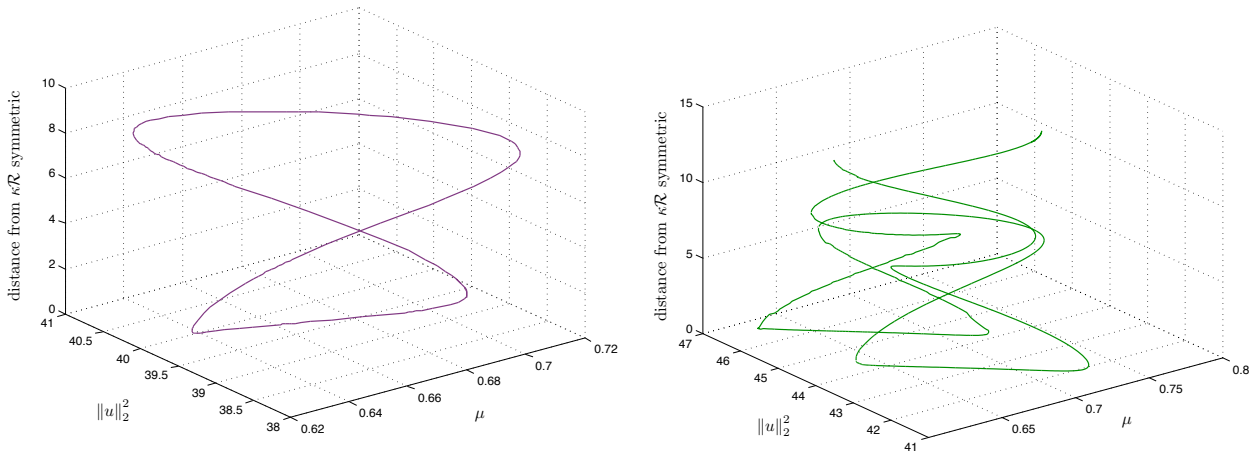

Figure 18: Left: *Another view of the isola found above, demonstrating that the symmetries are consistent with construction by combining a portion of the $\kappa\mathcal{R}$ symmetric solution branch with an asymmetric solution branch. The distance from $\kappa\mathcal{R}$-symmetry is computed as the L^2 norm of the difference between a given solution profile and the profile obtained by flipping across the y-axis, shifting by π in the x-direction, and multiplying by -1. Due to the approximate translation invariance of the solutions, this difference is minimized over translations in y.* Right: *A view of the cross-connecting branch found above, also consistent with construction via combination of $\kappa\mathcal{R}$-symmetric and asymmetric branches.*

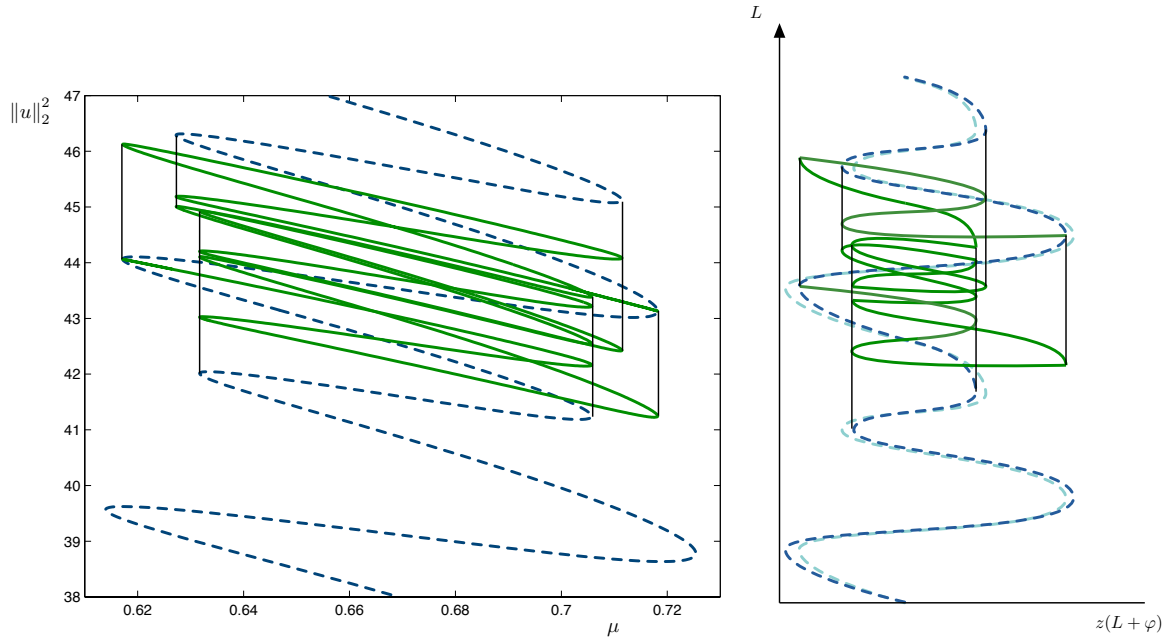

Figure 19: Left: *Partial bifurcation diagram for (5.3) with $\varepsilon = -0.01$, showing one of two $\mathcal{R}$-symmetric branches with $\varepsilon = -0.01$ in dashed blue, and a self-connecting asymmetric branch in solid green. Vertical lines indicate the correspondence between the saddle nodes of the $\mathcal{R}$-symmetric branch and of the self-connecting branch.* Right: *Reproduction of the predicted bifurcation diagram from Figure 14, with vertical lines showing alignments of saddle nodes, as in the numerically computed bifurcation diagram.*

5.2 Computation of splitting distance and comparison with continuation results

In their numerical study of symmetry-breaking in the one-dimensional cubic-quintic Swift–Hohenberg model, Houghton and Knobloch noted that the splitting distance is unequal on the left and right side of the snaking diagram; that is, the symmetry breaking term causes the set of saddle nodes to shift more to both the inside and outside on one side than on the other side.

To understand this observation, and to explain a similar phenomenon which occurs in the two-dimensional case – see Figures 16 and 19, in which the displacement of the outer saddle nodes on the left is much less than on the right – we can look at the derivative of the perturbed Swift–Hohenberg equation (2.1) or (5.2) with respect to ε. Starting with the one-dimensional case, we define

$$F(u, \mu, \varepsilon) := -(1 + \partial_x^2)^2 u - \mu u + bu^3 - u^5 + \varepsilon g(u)$$

where $g(u)$ is our perturbative term, e.g., u^2 or u_x^2. We can then parameterize a solution branch for the unperturbed system as $(u(s), \mu(s))$, where s is, for instance, arc length along the branch, so that

$$F(u(s), \mu(s), 0) = 0$$

for all s. We denote the tangent vector to this solution branch by

$$(v, \nu) := \frac{d}{ds}(u, \mu)(s).$$

For ε nonzero, the persisting $\mathcal{R}$-symmetric branch will be given by

$$F(u(s, \varepsilon), \mu(s, \varepsilon), \varepsilon) = 0,$$

and differentiating this with respect to ε we obtain

$$F_u u_\varepsilon + F_\mu \mu_\varepsilon + F_\varepsilon = 0.$$

Defining $\mathcal{L} = -(1 + \partial_x^2)^2 - \mu + 3bu^2 - 5u^4$ for a particular solution (u, μ), this yields the system

$$\begin{cases} \mathcal{L}u' - u\mu' + g(u) = 0 \\ \langle u', v \rangle + \mu'\nu = 0 \end{cases} \tag{5.4}$$

whose solution is $(u', \mu') = \frac{d}{d\varepsilon}(u, \mu)$. Thus the offset along the solution branch will be given by $\mu'\varepsilon + \mathrm{O}(\varepsilon^2)$. We can find μ' anywhere along the solution branch by solving the linear system (5.4). Alternatively, we note that, at a saddle node, we have $\nu = 0$ so that $\mathcal{L}v = 0$; since $\mathcal{L}$ is self-adjoint in L^2, applying $\langle v, \cdot \rangle$ to the first equation in (5.4) yields

$$\langle v, \mu' u \rangle + \langle v, g(u) \rangle = 0$$

or

$$\mu' = \frac{\langle v, g(u) \rangle}{\langle v, u \rangle}.$$

Thus we need only to calculate the solution (u, μ) and its associated eigenfunction v to compute the offset at a saddle node. While the method of directly solving the linear system is somewhat more robust numerically, the latter method provides helpful insight, particularly in the one-dimensional case.

We emphasize that, whichever method we use, this calculation allows us to determine the sign of $\tilde{Z}$ as defined in Section 4, which in turn determines which class of bifurcation diagram the perturbed system will exhibit; that is, we can describe the full bifurcation diagram without the need for any computations on the perturbed system.

In Figure 20 we show four successive saddle nodes for the one-dimensional cubic-quintic Swift–Hohenberg equation prior to perturbation. We see that the solution $u(x)$ at successive left-hand saddle nodes is related by

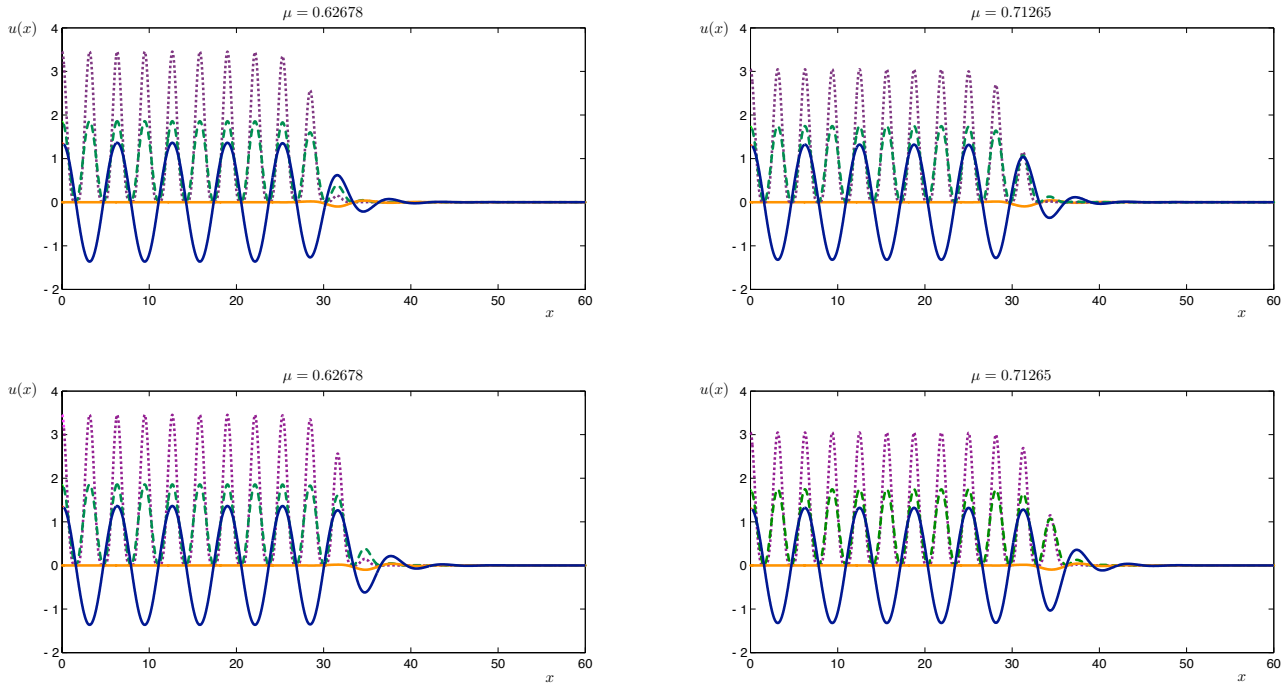

Figure 20: *Four successive saddle nodes, i.e., one full 2π-period along the snaking $\mathcal{R}$-symmetric branch, for the one-dimensional Swift–Hohenberg equation without perturbation. Solution $u(x)$ in solid blue, saddle node eigenfunction $v(x)$ in solid orange, $g(u) = u^2$ in dashed green and $g(u) = u^4$ in dotted purple.*

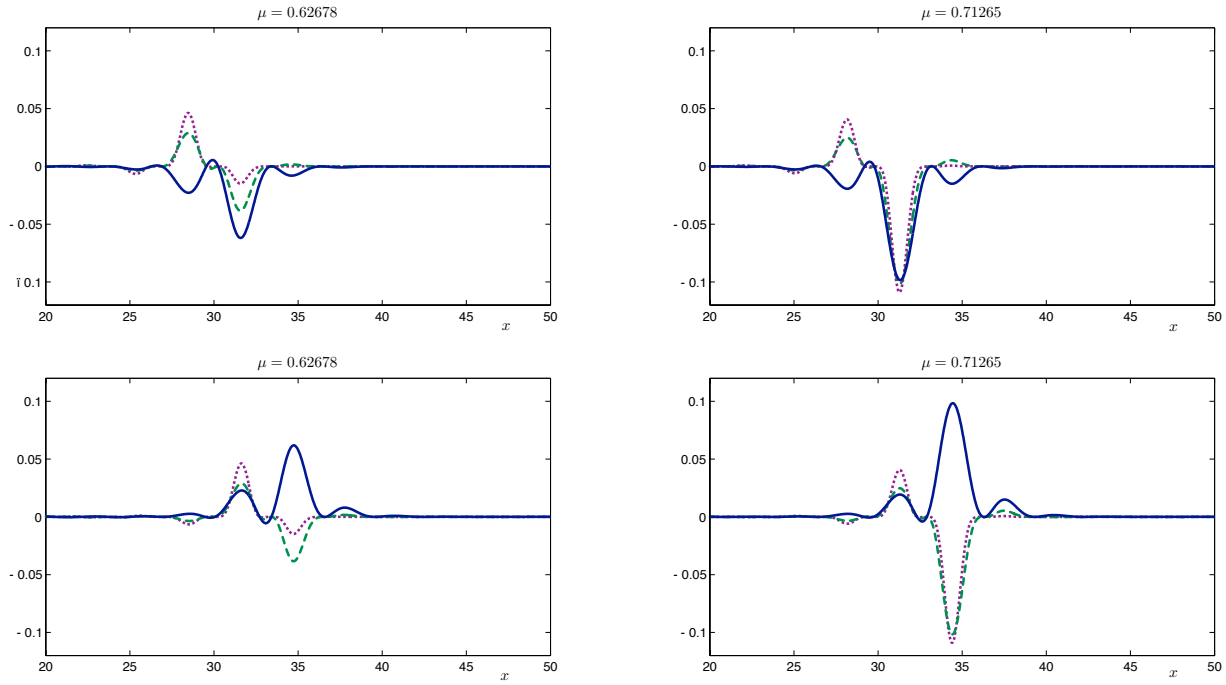

Figure 21: *The same four successive saddle nodes as in Figure 20, but now showing the pointwise product of the eigenfunction $v(x)$ with $u(x)$, $u^2(x)$, and $u^4(x)$. The function $(uv)(x)$ is shown in solid blue, $(u^2v)(x)$ in dashed green and $(u^4v)(x)$ in dotted purple.*

	$g(u) = u^2$		$g(u) = u^4$	
μ at saddle node	observed offset	calculated offset	observed offset	calculated offset
0.7084	-0.4472	-0.4322	-0.2996	-0.2833
0.6156	-0.0426	-0.0470	0.1667	0.1612
0.7218	-0.4713	-0.4668	-0.3581	-0.3585
0.6294	0.1231	0.1235	-0.2331	-0.2237
0.7084	0.4361	0.4269	0.2669	0.2883
0.6156	0.0611	0.0514	-0.1508	-0.1590
0.7218	0.4833	0.4669	0.3581	0.3575
0.6294	-0.1352	-0.1228	0.2083	0.2241

Table 1: *Observed and calculated offsets over 8 saddle nodes, i.e., a full 2π period of the function z, for the planar stripe and spot pattern of (5.1), with additional perturbative term $\varepsilon g(u)$ as indicated.*

$u \mapsto -u$ symmetry, and similarly on the right. We also graph the saddle node eigenfunction $v(x)$ and the perturbative terms $u^2(x)$ and $u^4(x)$. Recalling that the offset will be determined by the ratio of the inner product $\langle v, g(u)\rangle$ to $\langle v, u\rangle$, in Figure 21 we show the pointwise products of $v(x)$ with $u(x)$, $u^2(x)$, and $u^4(x)$. We observe that at the left saddle node, the peaks of $(u^2v)(x)$ and $(u^4v)(x)$ are approximately the same size, leading to a small value for $\langle v, g(u)\rangle$, which results in a smaller offset. On the other hand, for the saddle nodes on the right, u^2 and u^4 both exhibit a dominant peak, so that $\langle v, g(u)\rangle$ is of similar order to $\langle v, u\rangle$, resulting in a larger offset. The difference between the signs of the offsets for $g(u) = u^2$ and $g(u) = u^4$ is somewhat more subtle, though as we've noted already, in the one-dimensional case all offsets lead to qualitatively similar bifurcation diagrams.

For the two-dimensional case, we show in Table 1 the results of solving for μ' using the linear method: the observed offset is the difference between the original μ at the saddle node and that seen in the numerical continuation, divided by the ε used in the continuation; the calculated offset is the value of μ', computed by solving the linear system at a saved solution (u, μ) near each saddle node in the original $\varepsilon = 0$ bifurcation diagram. The values of ε used in the continuation were $\varepsilon = -0.0108$ for $g(u) = u^2$, and $\varepsilon = .01008$ for $g(u) = u^4$. We note that finer meshes (e.g., 16 Fourier modes instead of 8) and more accurate calculation of the saddle node locations lead to somewhat higher accuracy, but since there is already some difference in the absolute value of the offsets at successive saddle nodes at distance π, e.g., between the second and sixth saddle nodes in Table 1, there are nonlinear effects which would necessitate the inclusion of higher order derivatives in ε for a complete match. Nonetheless, we see that the agreement is quite good.

6 Discussion

In the preceding, we have shown that given a snaking system possessing a $\mathbb{Z}_2$ symmetry, we can predict on analytical grounds how the solutions and bifurcation structure will evolve in the presence of perturbative terms breaking the symmetry. These predictions cover the full bifurcation diagram, including the movement of symmetric branches and the reorganization of the $\kappa\mathcal{R}$-symmetric and asymmetric branches. They also explain the appearance and approximate symmetries of particular solutions lying along the new bifurcation branches. Furthermore, we have shown that given an appropriate form of the original system, isolas should form upon introduction of a particular perturbation. We then verified this numerically, and demonstrated that the isolas are formed exactly as expected, and possess the predicted approximate symmetries.

In addition, we have reiterated the observation of Houghton and Knobloch on the splitting distance of the symmetric branches, and provided an explanation based on the eigenfunctions in the one-dimensional case with which their paper was concerned. In fact, we have provided a method to calculate the splitting distances to

leading order in any dimension, and have shown that this method agrees well with the results of numerical continuation in the planar case. This method can be employed further to determine which perturbations lead to which bifurcation scenarios, using measurements from only the unperturbed bifurcation structure. Finally, we observe that this sort of analysis could be used to interpret or predict results of varying ν for various pattern types, some of which were reported in [2].

Several areas remain for future exploration. Although it seems clear at this stage, it has not yet been shown analytically that asymmetric solutions are constructed by gluing together symmetric solutions, even in the one-dimensional case. Proving this rigorously will aid in addressing the stability of planar patterns; while some computations have been done numerically, stability in the planar case has yet to be studied analytically. Beyond this, localized hexagon patches (see, for example, [18]) and other fully localized structures in two or higher dimensions remain challenging phenomena where even the bifurcation structures themselves remain poorly understood. Furthermore, as highlighted recently in [24], there are strong connections between the description of localized structures via Swift–Hohenberg-type models and the transition from a fluid to crystalline state; understanding these relationships promises to be a fruitful area for ongoing work.

Acknowledgements Makrides was supported by the NSF under the IGERT grant "Reverse Ecology: Computational Integration of Genomes, Organisms, and Environments" DGE-0966060. Sandstede was partially supported by the NSF under grant DMS-0907904.

References

[1] Y. Astrov and Y. Logvin. Formation of clusters of localized states in a gas discharge system via a self-completion scenario. *Phys. Rev. Lett.* **79** (1997) 2983–2986.

[2] D. Avitabile, D. J. B. Lloyd, J. Burke, E. Knobloch and B. Sandstede. To snake or not to snake in the planar Swift-Hohenberg equation. *SIAM J. Appl. Dyn. Syst.* **9** (2010) 704–733.

[3] M. Beck, J. Knobloch, D. J. B. Lloyd, B. Sandstede and T. Wagenknecht. Snakes, ladders, and isolas of localized patterns. *SIAM J. Math. Anal.* **41** (2009) 936–972.

[4] S. Blanchflower. Magnetohydrodynamic convectons. *Phys. A* **261** (1999) 74–81.

[5] U. Bortolozzo, M. G. Clerc and S. Residori. Solitary localized structures in a liquid crystal light-valve experiment. *New J. Phys.* **11** (2009) 093037.

[6] J. Burke and E. Knobloch. Localized states in the generalized Swift-Hohenberg equation. *Phys. Rev. E* **73** (2006) 056211.

[7] J. Burke and E. Knobloch. Homoclinic snaking: Structure and stability. *Chaos* **17** (2007) 037102.

[8] J. Burke and E. Knobloch. Snakes and ladders: localized states in the Swift-Hohenberg equation. *Phys. Lett. A* **360** (2007) 681–688.

[9] S. J. Chapman and G. Kozyreff. Exponential asymptotics of localised patterns and snaking bifurcation diagrams. *Phys. D* **238** (2009) 319–354.

[10] P. Coullet, C. Riera and C. Tresser. Stable static localized structures in one dimension. *Phys. Rev. Lett.* **84** (2000) 3069–3072.

[11] M. Cross and P. Hohenberg. Pattern formation outside of equilibrium. *Rev. Mod. Phys.* **65** (1993) 851–1112.

[12] H. Dankowicz and F. Schilder. An extended continuation problem for bifurcation analysis in the presence of constraints. *ASME J. Comp. Nonlin. Dyn.* **6** (2011).

[13] J. H. P. Dawes. The emergence of a coherent structure for coherent structures: localized states in nonlinear systems. *Philos. Trans. R. Soc. Lond. Ser. A Math. Phys. Eng. Sci.* **368** (2010) 3519–3534.

[14] M. F. Hilali, S. Metens, P. Borckmans and G. Dewel. Pattern selection in the generalised Swift-Hohenberg model. *Phys. Rev. E* **51** (1995) 2046–2052.

[15] S. M. Houghton and E. Knobloch. Swift-Hohenberg equation with broken cubic-quintic nonlinearity. *Phys. Rev. E* **84** (2011).

[16] J. Knobloch, M. Vielitz and T. Wagenknecht. Non-reversible perturbations of homoclinic snaking. *Nonlinearity* **25** (2012) 3469–3485.

[17] G. Kozyreff and S. J. Chapman. Asymptotics of large bound states of localized structures. *Phys. Rev. Lett.* **97** (2006) 044502.

[18] D. J. B. Lloyd, B. Sandstede, D. Avitabile and A. R. Champneys. Localized hexagon patterns of the planar Swift–Hohenberg equation. *SIAM J. Appl. Dyn. Syst.* **7** (2008) 1049–1100.

[19] D. Peterhof, B. Sandstede and A. Scheel. Exponential dichotomies for solitary-wave solutions of semilinear elliptic equations on infinite cylinders. *J. Differ. Eqns.* **140** (1997) 266–308.

[20] S. Pirkl, P. Ribière and P. Oswald. Forming process and stability of bubble domains in dielectrically positive cholesteric liquid crystals. *Liquid Crystals* **13** (1993) 413–415.

[21] Y. Pomeau. Front motion, metastability, and subcritical bifurcations in hydrodynamics. *Phys. D* **23** (1986) 3–11.

[22] H. Sakaguchi and H. R. Brand. Stable localized squares in pattern-forming nonequilibrium systems. *Europhys. Lett.* **38** (1997) 341–346.

[23] B. Sandstede and Y. Xu. Snakes and isolas in non-reversible conservative systems. *Dyn. Syst.* **27** (2012) 317–329.

[24] U. Thiele, A. Archer, M. Robbins, H. Gomez and E. Knobloch. Localized states in the conserved Swift–Hohenberg equation with cubic nonlinearity. Preprint (2013).

[25] P. D. Woods and A. R. Champneys. Heteroclinic tangles and homoclinic snaking in the unfolding of a degenerate reversible Hamiltonian-Hopf bifurcation. *Phys. D* **129** (1999) 147–170.